# POLITECNICO DI TORINO

Master's degree in Environmental and Land Engineering

Climate Change


Politecnico di Torino

# Field experiences of monitoring greenhouse gas emissions in the environment with FTIR and TDLAS techniques

Supervisors:

Prof. Rajandrea Sethi

Prof. Alessandro Casasso

Ing. Fabrizio Manassero

Candidate:

Luca Vivenza

Academic year 2022/2023

# Table of contents

# Foreword

Global warming is defined as the increase in the surface average temperature of the earth since the pre-industrial period (between 1850 and 1900) because of the increase, due to human activities, of the concentration of greenhouse gases such as water vapor, $CH_4$, $O_3$, $CO_2$, CFCs, and $N_2O$. The reduction of anthropogenic GHG emissions is therefore considered as the key to mitigate climate change.

This thesis is focused on the characterization of methane ($CH_4$) emissions, i.e., the second largest anthropogenic GHG in terms of radiative forcing after $CO_2$. In particular, this gas has a global warming potential (GWP) of 29 over a 100-years horizon, whereas its GWP over a 20-years horizon is 82. This is due to its relatively short life in the atmosphere and makes it particularly important to reduce $CH_4$ emissions to mitigate climate change in the short term.

There is a need to develop and improve methods for the characterization of $CH_4$ emissions and, at present, standardized methodology to detect methane emissions are lacking in several sectors, especially major sources like municipal solid waste landfills, biogas plants and manure storages. This thesis presents applications of FTIR and TDLAS for methane emissions estimation in two case studies, i.e., an anaerobic digestion plant and a municipal solid waste landfill.

The thesis is structured as follows. Chapter 1 deals with the description of the behaviour of GHGs in atmosphere, with the political actions that EU is taking and with the most commonly used emission measurement techniques. Chapter 2 describes the results of a measurement campaign conducted in a small biogas plant located in the province of Cuneo. Chapter 3 describes the results of a measurement campaign conducted in a municipal solid waste landfill placed in the province of Asti.

Chapter 4 reports the conclusions of the work, along with possible future developments.

# 1 Introduction

## 1.1 Global Warming and anthropogenic greenhouse gas (GHG) emissions

Global warming is defined as the increase in the surface average temperature of the earth since the pre-industrial period (between 1850 and 1900) because of the increase, due to human activities, in the concentration of greenhouse gases such as water vapor, $CH_4$, $O_3$, $CO_2$, CFCs, and $N_2O$.

The main causes can be identified in the burning of fossil fuels for heating, cooling, transportation and electricity.

The last report provided by the IPCC (2021, [1]) starts with the following sentence: "It is unequivocal that human influence has warmed the atmosphere, ocean, and land. Widespread and rapid changes in the atmosphere, ocean, cryosphere, and biosphere have occurred". From these words it is evident that global warming and the consequent climate change is one of the biggest challenges that mankind must face. Moreover, in a special report provided once again by IPCC (2018, [2]), it is explained that Earth has warmed between 0.8 and 1.2 °C since 1750.

Some indicators of the alteration of climate because of global warming are:

- More extreme weather events
- Melting of Artic Sea ice
- Land ice behaviour
- Weather pattern changes
- Biodiversity losses and changes
- Rising sea levels
- Ocean acidification

### 1.1.1 Greenhouse gas effect

As already said, global warming is caused by the increase of the concentration of GHGs in atmosphere, but greenhouse gas effect is a natural phenomenon. Without it, the temperature of the earth surface would be too low to allow the development of life (it would be around -18 °C). The problem arises when the concentration of these gases increases, because it means that the amount of heat trapped in the atmosphere increases (and so the temperature, with consequences over all the ecosystems) [3].

The GHG with the highest concentration in the atmosphere is the water vapor, which has a concentration in the order of a hundred time higher than $CO_2$ and contributes around 60% to the global warming effect. The amount of water vapor depends on temperature and temperature depends on the concentration of GHGs. For these reasons an increase of concentration of GHGs would cause an increase of the global temperature that would cause an increase in the water vapor concentration (because of a higher evaporation from the ocean). Water vapor is the only one GHG affected by condensation. All the

others are not because they are all well-mixed gases that don't react to changes in temperature or pressure [4]. Those GHGs have increased their concentration in the atmosphere. In particular, the report of IPCC provides many data on the variation of these gases. For example, the concentrations of three important GHGs in 2019 were (IPCC, 2021 [1]):

- $CO_2$: 410 ppm (19 ppm more than 2011)
- $CH_4$: 1866 ppb (63 ppb more than 2011)
- $N_2O$: 332 ppb (8 ppb more than 2011)

Moreover, Figure 1 shows the concentration of these three important greenhouse gases since from 800,000 years ago.

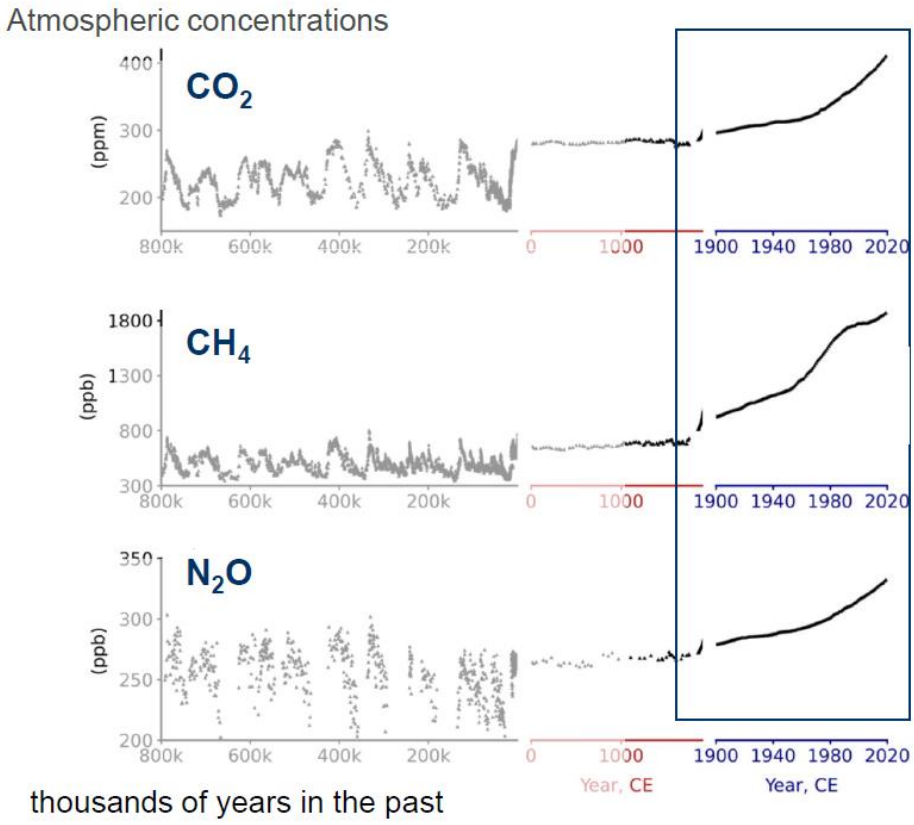


*Figure 1 - Variation of concentration of GHGs [1].*

The sixth report of IPCC highlights that each of the last four decades has been warmer than any decade that preceded it since 1850. Global surface temperature was 1.09 (0.95 to 1.20) °C higher in 2011-2020 than 1850-1900. Moreover, it is considered very likely that well-mixed GHGs were the main driver of tropospheric warming since 1979. In 2019, atmospheric $CO_2$ concentrations were higher than at any time in at least 2 million years, while concentrations of $CH_4$ and $N_2O$ were higher than at any time in at least 800,000 years. Since 1750, the increase in $CO_2$ and $CH_4$ have been respectively 47% and 156%. Human-caused radiative forcing of 2.72 (1.96 to 3.48) W/m$^2$ in 2019 relative to 1750 has warmed the climate system. This has been caused mainly by the increase of GHG concentrations. [5]

Moreover, the evidence that the $CO_2$ rising is caused by human activity can be found in the relative ratios of carbon isotopes. The amount of $^{13}C$ in the atmosphere has been declining because of the ratio of $^{13}C$ in the $CO_2$ from fossil fuels is lower than the $CO_2$ coming from the decaying plants.

The reason why GHGs have an important role in warming the planet can be found in their molecular structure. GHGs are composed by three or more atoms which are bound loosely enough together to be able to vibrate with the absorption of heat. This structure makes them possible to trap heat in the atmosphere and then transfer it to the surface of the earth. This cycle causes an overall increase in global temperatures if the amount of total GHGs is increased, as shown in Figure 2. They can absorb and then radiate the infrared radiation [5].

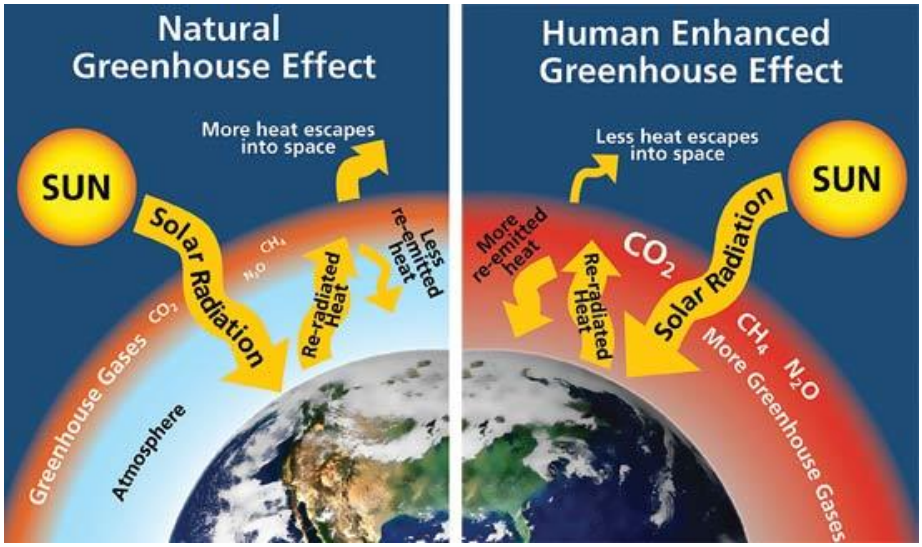


*Figure 2 - Representation of the effects of the increasing of concentration of GHGs [4].*

The solar radiation spectrum is based on three main ranges of wavelength: ultraviolet, visible, and infrared. About half of the radiation is in the visible part of the electromagnetic spectrum. The UV range accounts for the 7-8% of the total, but it is very important because of the high energy content. The rest of the energy is spread over the wavelengths longer than the visible light. The atmosphere is transparent to the visible light (short wavelength), that is absorbed by the surface of the earth and then re-emitted in the form of invisible infrared radiation, that will be absorbed by the GHGs. [3]

Greenhouse gas emissions come from a huge number of sectors. For example, in the year 2016 the global GHG emissions were 49.4 billion of tons of $CO_2$ equivalent and they were divided as reported in the Figure 3. The most relevant problem is referred to the energy needs, that caused the 73.2% of the total emissions. [6]

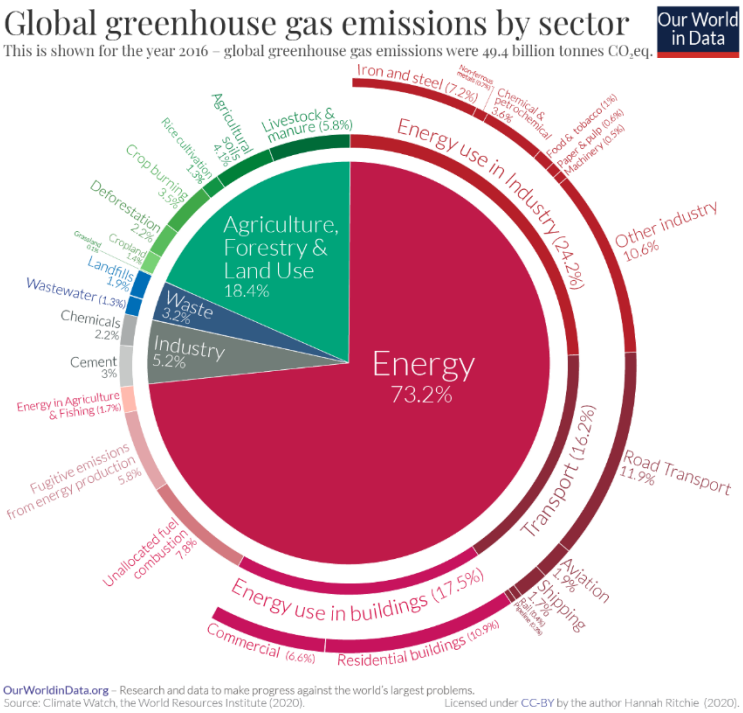


*Figure 3 - Global GHG emissions by sector in the year 2016. Source: bit.ly/GHGs_emissions_OWD [6].*

Still referring to the year 2016, it is also possible to analyse the percentage of emission of the GHGs, as shown in Figure 4.

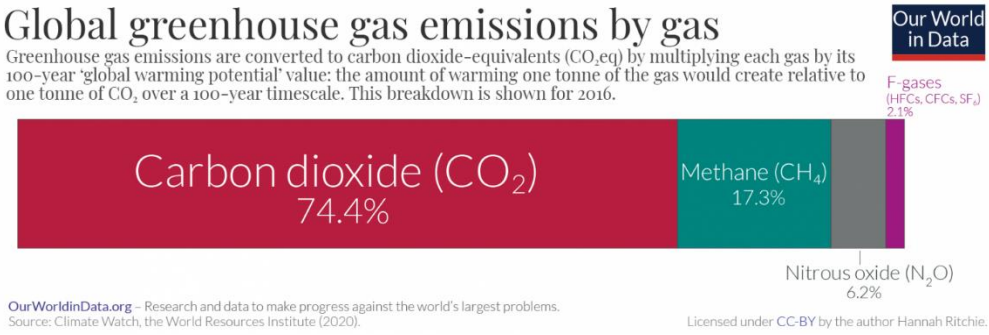


*Figure 4 - Emissions by gas for the year 2016. Source: bit.ly/GHGs_emissions_OWD [6].*

### 1.1.2 Global Warming Potential

To compare the effect of the different greenhouse gases, the global warming potential of each gas must be considered. It is a measure of how much energy the emissions of one ton of a gas will absorb over a certain period, relative to the emissions of one ton of $CO_2$. The larger the GWP, the higher is the warming effect of a gas. Usually, the time considered is 100 years. This measure allows the comparison of the different greenhouse gases. The GWP of $CO_2$ is equal to 1. Methane has a GWP over a timeframe of 100 years equal to 27-30. Methane lifetime in the atmosphere is much lower than carbon dioxide, but $CH_4$ absorbs much more energy than $CO_2$. $N_2O$ has a GWP of 273 over 100 years. Figure 5 resumes some famous greenhouse gases and their GWP over a timeframe of 20, 100 and 500 years.

| # Species | Lifetime (years) | Radiative efficiency (W $m^{-2}$ $ppb^{-1}$) | GWP-20 | GWP-100 | GWP-500 |
|---|---|---|---|---|---|
| CO2 | Multiple | $1.33\pm0.16 \times 10^{-5}$ | 1. | 1.000 | 1.000 |
| $CH_4$-fossil | 11.8 ±1.8 | $5.7\pm1.4\times10^{-4}$ | 82.5 ±25.8 | 29.8 ±11 | 10.0 ±3.8 |
| $CH_4$-non fossil | 11.8 ±1.8 | $5.7\pm1.4\times10^{-4}$ | 80.8 ±25.8 | 27.2 ±11 | 7.3 ±3.8 |
| $N_2O$ | 109 ±10 | $2.8\pm1.1 \times10^{-3}$ | 273 ±118 | 273 ±130 | 130 ±64 |
| HFC-32 | 5.4 ±1.1 | $1.1\pm0.2 \times10^{-1}$ | 2693 ±842 | 771 ±292 | 220 ±87 |
| HFC-134a | 14.0 ±2.8 | $1.67\pm0.32 \times10^{-1}$ | 4144 ±1160 | 1526 ±577 | 436 ±173 |
| CFC-11 | 52.0 ±10.4 | $2.91\pm0.65 \times10^{-1}$ | 8321 ±2419 | 6226 ±2297 | 2093 ±865 |
| PFC-14 | 50000 | $9.89\pm0.19 \times10^{-2}$ | 5301 ±1395 | 7380 ±2430 | 10587 ±3692 |

*Figure 5 - Greenhouse gases and relative values of GWP [1].*

### 1.1.3 European political actions to reduce methane emissions

Methane is a powerful GHG, second only to $CO_2$ in the overall contribution to climate change.

It contributes to tropospheric ozone formation and causes health problems.

Reducing $CH_4$ emissions contributes to slowing down climate change and improving air quality.

Current European policies are projected to reduce methane emissions by 29% in 2030 compared to 2005 levels. At global level, reducing the emissions by 50% in the next 30 years could reduce the temperature change by 0.18 °C.

Approximately, the $CH_4$ emissions worldwide can be resumed as:

- 41% from natural sources, like wetlands or wildfires
- 59% from anthropogenic activities. These emissions can be furthermore divided in several sectors:
    - Agriculture (40-53%)
    - Fossil fuel production and use (19-30%)
    - Waste (20-26%)

The EU deals with methane reduction strategies since 1996. Relative to 1990 levels, the methane emissions in some key sectors have fallen respectively by:

- 1/2 in energy sector
- 1/3 in waste management
- 1/5 in agriculture

In energy sector, 54% of methane emissions are fugitive emissions from oil and gas sector, 34% from the coal sector and 11% from residential or other sectors. The EU's climate target plan impact assessment indicates that the most cost-effective methane emissions reduction can be achieved in the energy sector.

In the agricultural sector, the reduction in emissions passes through the reduction of nutrient losses in animal feed and through the production of biogas. The emissions from livestock are due mainly to ruminant species (80%), manure management (17%) and rice cultivation.

In the waste sector, the main source of methane emissions are the uncontrolled emissions of gas from landfills. Other source of emissions are the treatment of sewage sludge and leaks from biogas plants. In Europe, between 1990 and 2017 the emissions from landfill have been already reduced by 47% thanks to a better compliance with EU waste legislation of emissions from landfill. This achievement has been reached thanks to the development of other waste-treatment options for biodegradable wastes, such as composting and anaerobic digestion, and to the stabilization of biodegradable wastes before the disposal. It is expected to develop more stringent compliance practices to have a stronger reduction of methane emissions from wastes [7].

One of the main objectives of the EU actions is to ensure that companies apply accurate measurements and reporting methodologies for methane emissions, to better understand the problems and to develop mitigation actions.

The United Nations Framework Convention on Climate Change (UNFCCC) has a three-tier reporting framework for methane emissions, which can be applied across all the emitting sectors:

Tier 1 is the most basic approach, involving simple estimations based on activity data and emission factors.

Tier 2 may combine elements of both Tier 1 and Tier 3

Tier 3 is the most complex one, both in terms of data requirements and methodological complexity.

The Tier level applied varies between countries and only few members of EU apply Tier 3 standards. It is expected to see an increase in the number of nations that apply a Tier 3 approach in many sectors.

In energy sector, thanks to the adoption of the framework developed under the Climate and Clean Air Coalition Oil and Gas Methane Partnership, the increasing in the precision of the calculation of emissions will be expected in the next few years.

In agricultural sector, the Tier 2 approach is momentarily considered sufficient because of the huge number of actors involved in the processes. However, the final objective must be the adoption of Tier 3.

In the waste sector, the quality of data is already robust for waste disposal in landfills [7].

Currently, there are not present international bodies which collect and verifies methane emissions data. Europe Commission will support the establishment of an independent and international methane emissions observatory. Its objective will be the collection, verification and publication of data related to the global anthropogenic emissions of methane. Moreover, a section dedicated to the development of new testing and monitoring technologies will be implemented.

Moreover, the EU's Copernicus program is contributing to improve indirect air surveillance and the monitoring of methane emissions. This approach is very effective in case of super-emitters (specific site or facility with disproportionately high emissions for a site or facility of that kind). In 2025, when the Copernicus $CO_2$-monitoring mission will be launched, the identification of smaller and more prevalent sources of emissions will be supported, and it will be possible to monitor the global atmospheric $CH_4$.

In addition, the use of drones makes possible to survey large amounts of infrastructures in a very cost-effective way. This approach makes possible to increase the frequency of the aerial monitoring, that is a key point to address intermittent leaks.

In the European Green Deal, the Commission announced that it would review EU legislation, with the aim of delivering increased climate ambition as contained in the 2030 climate target plan assessment. Several pieces of legislation are within the scope of this review which have a bearing on methane emissions. This includes the EU Emissions Trading System (ETS) and the Effort Sharing Regulation (ESR), the latter covering all methane emissions in the EU next to all other greenhouse gases not covered by the emissions trading system. The assessment supporting the 2030 climate target plan underlined that also for these gases increased incentives will be required to reduce emissions further. The achievement of this strengthening of ambition will benefit from the sectoral actions in this strategy.

EU commission also believes in the opportunities coming from biogas production. In particular, agricultural and non-recyclable wastes can be used in anaerobic digesters to produce biogas or in biorefineries to produce bio-chemicals and biomaterials. Biogas is a source of renewable energy highly sustainable, with multiple applications. Moreover, materials from the anaerobic processes can be used as soil improver. According to the EU's long term decarbonization strategy, in 2050 the annual consumption of biogases will be between 54 and 72 Mtoe (in 2017 it has been 17 Mtoe). Biogas is also considered a cost-effective mitigation action in agriculture and waste sectors [7].

## 1.2 GHG emissions measurement techniques

Nowadays, several measurements techniques to detect GHGs (in this case mainly $CH_4$) are available, but none of them has been recognised as an international reference method. For this reason, depending on the type of site that must be analysed, each technique can be considered valid.

### 1.2.1 Surface flux chamber

The gas escaping from a surface is captured inside a chamber. Then, its variation of the concentration is measured. There are two main setups for this approach: open chamber or close chamber. Figure 6 shows the idea behind both concepts.

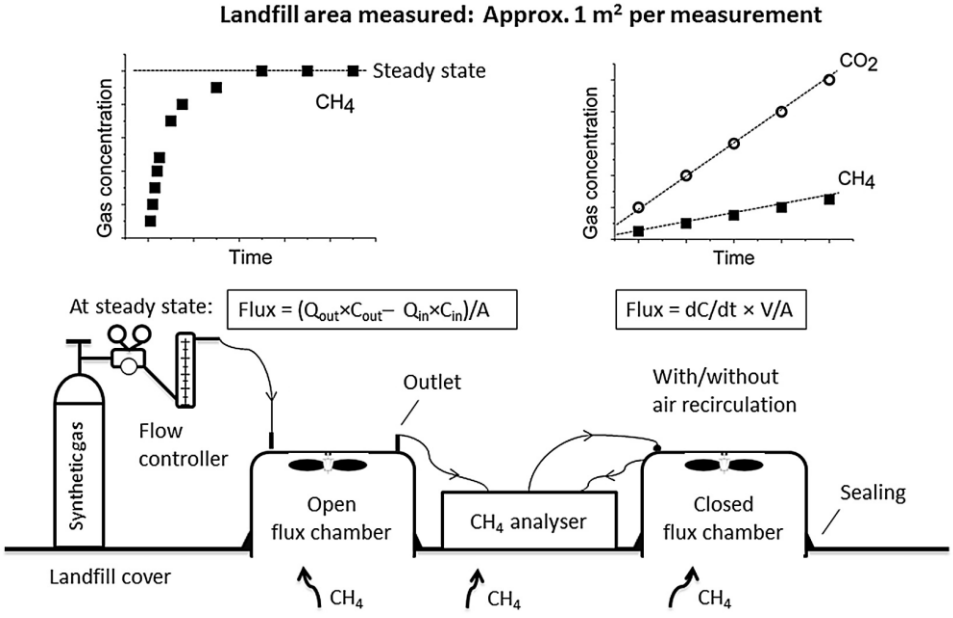


*Figure 6 - Open and closed chambers [8].*

Closed surface flux chambers (or static chambers) are a very common approach in many fields, such as in the detection of $CH_4$ emissions from wetlands or landfills (in this case they are considered the most common method to estimate $CH_4$). They can be set up with or without recirculating the gas. In case of a large volume taken from the chamber by the analyser, the recirculation is preferable. Often, chambers are equipped with tools that ensure the complete mixing of the gases inside the chamber.

The flux emissions of $CH_4$ from the surface covered by the chamber is calculated starting from the variation of the concentration inside the chamber:

$$Flux = \frac{dC}{dt} \cdot \frac{V}{A}$$

*Equation 1*

Where dC/dt is the variation in concentration over time, V is the volume of the chamber and A the surface that the chamber covers.

The size of the chamber can vary in a wide range, from less than 0.1 $m^2$ [9] to more than 15 $m^2$ [10].

Measurements are often performed over a short time (few minutes) to minimize the errors from the increase in pressure inside the chamber.

To measure the entire landfill emissions, chambers position can be defined randomly or through a systematic grid of single-point measurements. The total emission will be then measured calculating the average emissions coming from the chambers and multiplying it by the entire surface of the landfill.

Advantages and disadvantages of this approach are resumed in the Table 1.

*Table 1 - Closed surface flux chambers*

| Advantages | Disadvantages |
|---|---|
| Simple to employ | Low spatial resolution (between 0.5 and 1 $m^2$) |
| Doesn't require advanced equipment | Low temporal resolution (few minutes) |
| Only method available to define the flux of trace gases contained in landfill gases (LFG) | Underestimation of emissions because of low probability to capture hotspots |
| It can detect and quantify $CH_4$ oxidation at a location, if combined with proper methods | The chamber should be sealed. The process is complicated in case of presence of vegetation |
| | The flux can be underestimated because of the increase in pressure into the chamber |

Open flux surface chambers (or dynamic chambers) have a similar approach to static chambers, but in this case the chamber is continuously flushed with air. In this way the errors coming from the increase in pressure or concentration are removed and the measurements can be performed over a longer period. Pressure should be maintained at a value close to the one in the ambient. The emission rate is obtained by using the flow through the chamber and the concentrations at the inlet and outlet.

Advantages and disadvantages of this approach are resumed in the Table 2

*Table 2 - Open surface flux chamber*

| Advantages | Disadvantages |
|---|---|
| Low risk of overpressure inside the chamber | Need to use a synthetic gas as a carrier to guarantee constant conditions |
| Higher temporal resolution than static chambers | Setup more complicated than static chambers |

In conclusion, the flux chamber approach is not suitable for the total quantification of $CH_4$ emissions but can be an important tool to obtain the emission rate for smaller scale studies (e.g., comparison between covered or non-covered cells in a landfill).

### 1.2.2 Eddy covariance method

This approach is based on the fact that emitted gases are mixed vertically by turbulent eddies. Continuous measurements of the vertical gas mass fluxes are performed. Emissions can be obtained

starting from the concentrations of $CH_4$ and the local vertical wind velocity and they are usually calculated performing an average of the data over a defined period (like 15 minutes).

Measurements are taken on tower with a height between 0.5 and 10 m from the ground. The radius of the contributing area is usually 100 times higher than the height of installation. The source area is estimated through a dispersion model.

Advantages and disadvantages of this approach are resumed in the Table 3. In conclusion, this method can be applied in case of landfill with flat surfaces and homogeneous emissions.

*Table 3 - Eddy covariance method*

| Advantages | Disadvantages |
|---|---|
| Continuous measurements over a long period (months) of both $CH_4$ and $CO_2$ | Topography should be flat |
| It can provide an integrated measure of landscape-scale fluxes | Covered area is function of the wind speed |

### 1.2.3 Stationary mass balance method

Concentrations are measured over the surface at different heights. The horizontal flux is calculated through the comparison between the wind velocity and the measured concentration. The flux represents the emissions from the site upwind of the sampling point.

This method is considered only 1D because the flux passes through the tower and not through a larger vertical plane. A simple representation is shown in Figure 7.

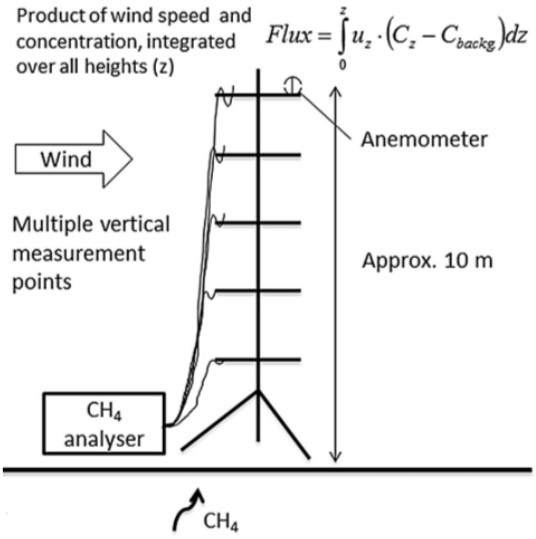


*Figure 7 - Stationary mass balance method [8].*

The background concentration is measured at the top of the tower. This procedure is performed to avoid overestimation of the results.

The considered area of the site is function of the height of the tower. If its maximum height is assumed to be 10 m, the contributing area will have approximately a radius of 150 m [11].

The specific size and location of the area where emissions are measured is defined by dispersion models. For this reason, it is also necessary to know the surrounding topography and the atmospheric conditions.

The area also depends on the wind: if it changes direction, the contributing area will change, giving the possibility to provide emissions rates from different areas of the site.

Advantages and disadvantages of this approach are resumed in the Table 4.

*Table 4 - Stationary mass balance method*

| Advantages | Disadvantages |
|---|---|
| Continuous measurements over a long period (months) of both $CH_4$ and $CO_2$ | Covered area is limited and it is function of the wind speed |
| | Topography should be flat |
| | Overestimation of results if there is a hotspot close to the tower |

### 1.2.4 Radial plume mapping

Radial plume mapping (RPM) takes advantage of the combination of wind profiles and concentration measurements to get a surface emission factor from an upwind area. This approach is considered a mass balance method. There are two possible configurations, shown in Figure 8:

- Horizontal (HRPM): it provides qualitative information on the location of hotspots
- Vertical (VRPM): it is used to quantify emissions

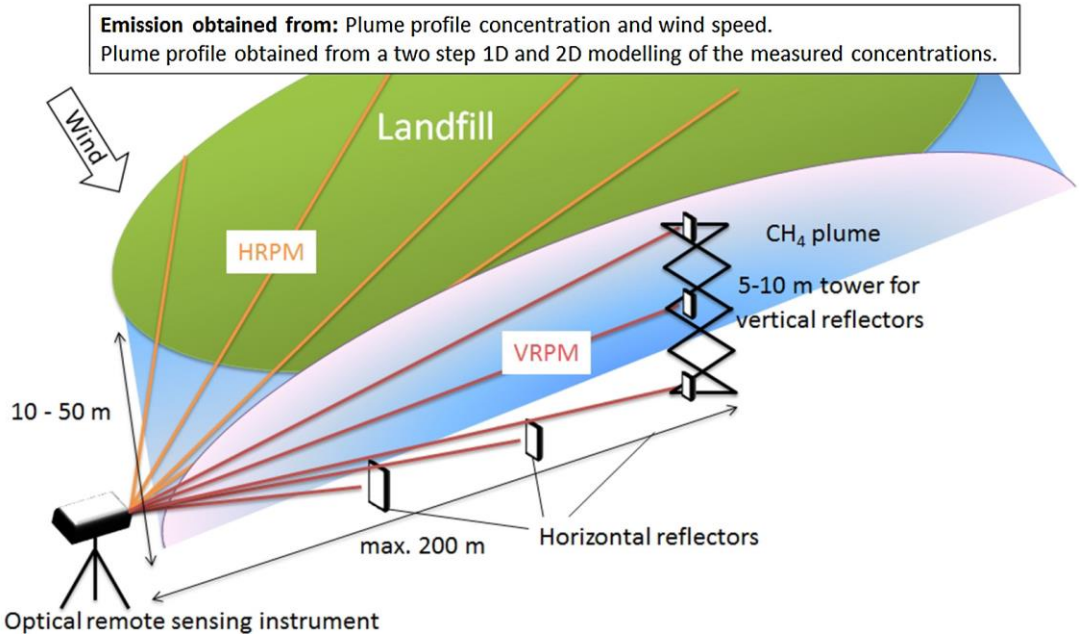


*Figure 8 - Scheme of both vertical and horizontal radial plume mapping [12].*

Emissions through the VRPM configuration are quantified measuring the mass of $CH_4$ crossing two vertical planes located upwind and downwind the desired area. Fluxes across the vertical planes are determined from the product of the wind velocity and the concentrations in the air. $CH_4$ emissions are obtained through the difference between the flux of the downwind plane and the flux of the upwind plane.

If the concentration in the upwind plane can be assumed constant, it is considered as the background concentration and the $CH_4$ flux can easily be calculated as the product of the wind velocity and the difference between downwind and upwind concentrations.

Thanks to the use of reflectors positioned at different heights and distances it is possible to get multiple laser beam paths from a single laser beam. The position of laser and reflectors must be as close as possible to the site. Each beam path (which length is usually up to 300 m) provides an average concentration of $CH_4$. Starting from these values, a cross-section concentration profile of the plume is modelled and a 2D concentration profile is obtained.

Advantages and disadvantages are resumed in the Table 5.

*Table 5 - Radial plume mapping*

| Advantages | Disadvantages |
|---|---|
| Gives an integrated measure of $CH_4$ emissions from the area upwind of the laser | Two lasers should be used. If only one laser is used, an inverse dispersion model is needed |
| Able to detect hotspots | Topography should be flat |
| | Only a part of the site is represented because of the limited range of the laser |

### 1.2.5 Tracer gas dispersion method

This method uses a tracer gas released at a known rate and the measurements of atmospheric $CH_4$ concentrations. It is assumed that $CH_4$ and the tracer gas have the same behaviour in the atmosphere during the entire measurement campaign. A schematization can be seen in Figure *9*.

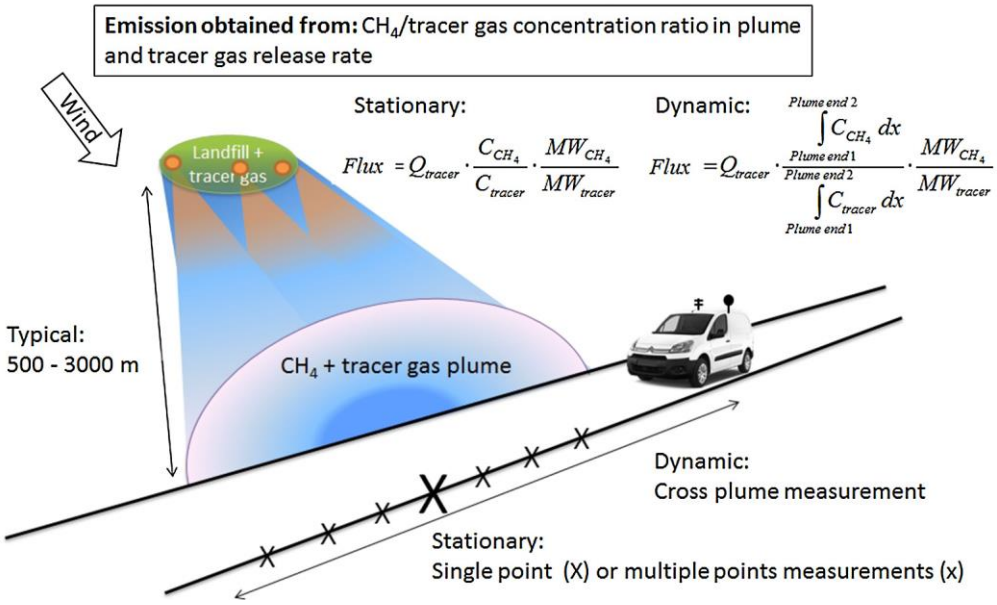


*Figure 9 - Tracer gas dispersion method [8].*

Nowadays the most common tracer is the acetylene ($C_2H_2$). Even if it is highly flammable, it is cheap, easy to be released at a constant rate and with a low GWP.

It is possible to follow two different approaches: stationary or dynamic approach.

In case of stationary approach, measurements are performed downwind from the emission source at fixed points in the plume. Before conducting the measurements, it is possible to locate the plume through analysers placed on vehicles. After that, multiple measurement points are placed across the plume to sample the air. measurements must be performed far enough from the site to guarantee a good mix between the tracer and $CH_4$. The correct distance is function of the size of the source, on the topography of the area and on the atmospheric conditions.

Advantages and disadvantages are resumed in the Table 6.

*Table 6 - Static tracer gas dispersion method*

| Advantages | Disadvantages |
|---|---|
| The whole emissions of the site are measured | It is difficult to locate the plume |
| | Wind conditions must be stable |

In case of dynamic approach, transects of the downwind plume are performed to measure the concentration of both tracer and $CH_4$ close to the ground and across the whole plume through the integration of subsequent plumes. This method requires measurements able to perform fast measurements.

Advantages and disadvantages are resumed in the Table 7.

*Table 7 - Dynamic tracer gas dispersion method*

| Advantages | Disadvantages |
|---|---|
| The whole emissions of the site are measured | The mixing depends on weather conditions |
| Doesn't depend on the topography | Expensive method and skilled operators required |
| Easy analysis and calculation after the mixing of tracer and $CH_4$ | Road at a suitable distance is needed |

### 1.2.6 Mass balance using aerial methods

It is possible to use both UAVs and aircrafts. The concentration of $CH_4$ is measured across the downwind plume at various heights. Usually, the entire height and width of the plume is covered.

The objective is to obtain a 2D concentration plane. It will then be combined with the measurement of wind speed and direction for calculating the $CH_4$ flux through the downwind plane (with consequent definition of the landfill emissions).

UAV is combined with instruments that have a sensitivity lower than the ones that can be carried on an aircraft. For this reason, UAV must measure closer to the site than the aircraft.

Advantages and disadvantages of this approach are resumed in the Table 8.

*Table 8 - Mass balance using aerial methods*

| Advantages | Disadvantages |
|---|---|
| The whole emissions of the site are measured | Accurate weather data required |
| | Closely located sites can be difficult to separate |

### 1.2.7 Inverse dispersion modelling

This method is based on the measurements of downwind concentrations. These measurements are combined with the meteorological data in order to calculate the emission rate from a source. This procedure is performed through the theory of gas dispersion in the atmosphere. Inverse modelling can be stationary or dynamic.

In the first case, one or more measurement points are defined. They must be downwind the landfill and they can recorder data continuously or for a fixed period. Many models have been developed using this approach (e.g., AERMOD, LASAT, WindTrax etc.), but all of them have in common the need of information about the shape of the surface, the wind speed and direction and the precise position of the measurements. Advantages and disadvantages are resumed in the Table 9.

*Table 9 - Inverse dispersion modelling: stationary*

| Advantages | Disadvantages |
|---|---|
| Long time series can be performed | Strong dependency on wind direction |
| The whole emissions of the site are measured | Sensitive to complex topography |
| | Complex data treatment |

The dynamic approach is also based on the measurements of downwind concentrations. It is equivalent to the dynamic tracer dispersion model, but it is performed without tracer.

The measured concentration profiles are used together with wind data to calculate the emissions data from the source thanks to a model.

Measurements are usually performed at a distance between 500 m and several kilometres from the landfill. At a sufficient distance the landfill can be seen as a single-point source (important assumption if a Gaussian model is applied), but the higher is the distance and the higher is the need to use very sensitive instruments able to detect variations of concentration of ppb.

Advantages and disadvantages are resumed in the Table 10.

*Table 10 - Inverse dispersion modelling: dynamic*

| Advantages | Disadvantages |
|---|---|
| The whole emissions of the site are measured | Need of precise and fast instrumentations |
| Measurements are fast | Weather parameters must be very detailed |

### 1.2.8 Differential absorption LiDAR (DIAL)

It is a laser-based technique which allows the measurement of methane concentration along an open path. The laser operates alternately at two adjacent wavelengths (they are chosen depending on the target gas). The first wavelength (defined as “on” wavelength) is set to the absorption line of the target gas (in this case $CH_4$), while the other one (defined as “off” wavelength) is set to minimize the absorption from the target gas. The concentration of methane is then measured through the difference between the “on” and “off” signals [13].

Measurements are performed along different lines in a vertical plane to obtain a 2D map of the gas concentration. The emission rate is calculated combining the 2D map with the vertical wind profile.

Advantages and disadvantages of this approach are resumed in the Table 11.

*Table 11 - DIAL*

| Advantages | Disadvantages |
|---|---|
| The whole emissions of the site are measured | Expensive technology |
| Provides detailed information on emission patterns | Wind parameters must be very accurate |
| Little interferences from other $CH_4$ sources around the site | Complex processing of data |

### 1.2.9 Vertical soil gas concentration profile

This approach can be used in landfills. Soil gas probes are inserted into the landfill top cover. The lowest part of the probe has slits that allow the gas to enter. Measures are taken at different depths of the

cover and sometimes also in the upper part of the waste. From samples it is possible to get the pore gas composition.

Soil gas profile provides qualitative information on the oxidation of $CH_4$, on the distribution of the gas and on its transport processes. For example, the concentration gradients of methane and carbon dioxide can give information about the area and the depth in which oxidation of $CH_4$ is occurring [14].

This method could bring to an overestimation of $CH_4$ oxidation because processes such as soil respiration produce $CO_2$. To reduce this problem, it should be performed a background analysis on areas without landfill gas exposure to assess a background value of soil respiration.

This approach is often combined with soil sampling at the respective depths of the cover. The objective is to define in laboratory the $CH_4$ oxidation potential of the cover soil.

Advantages and disadvantages of this method are resumed in the Table 12.

In summary, this approach has limited application as a standalone method for quantifying landfill gas (LFG) emissions but can become very useful if combined with other quantitative emission methods.

*Table 12 - Vertical soil gas concentration profile*

| **Advantages** | **Disadvantages** |
|---|---|
| Useful to study the influence of atmospheric pressure changes on $CH_4$ emissions | Low spatial resolution (sampling area is usually lower than 0.5 $m^2$) |
| Useful to understand the direction of the diffusional flux of $CH_4$ | Low temporal resolution (no more than 20 minutes) |

## 1.3 GHG measurement equipment

The number of possible technologies to measure GHG is very large. Since this thesis focuses on Fourier Transform Infrared Spectroscopy (FTIR) and Tunable Diode Laser (TDLAS).

### 1.3.1 Fourier Transform Infrared Spectroscopy (FTIR)

FTIR (Fourier Transform InfraRed) spectroscopy is the most popular analytical technology for industrial applications requiring the continuous measurement of multiple parameters simultaneously. FTIR analysers are usually employed for process control and emissions monitoring, but they can also be used for a wide range of activities. Some advantages of this technique can be found in the rapidity of the measurement (to acquire one spectrum few seconds are needed), in the high precision and in the absence of process of sample pre-treatments. Moreover, no daily routine calibration is required.

FTIR gas analysers identify and measure gaseous compounds through the absorbance of infrared radiation. This can be done thanks to the fact that each molecular structure has a different combination of atoms from the others, and therefore produces a unique spectrum when exposed to infrared light. The analysis of the spectrum allows a qualitative and quantitative identification of the gas. The infrared spectrum is a plot of infrared radiation related quantities as a function of wavelength or wavenumbers.

On the x-axis there can be present the wavelength expressed in µm or more commonly the wavenumber expressed in $cm^{-1}$ (for example if the wavelength is 500 µm, the wavenumber will be equal to 20 $cm^{-1}$). According to the Lambert-Beer Law, the absorbed light is directly proportional to the concentration of the gas at a constant width. Thanks to this relationship, it is possible to define the concentration of the compounds in a sample gas from the infrared light absorbance.

Diatomic elements such as $N_2$ and $O_2$ and noble gases can't be detected.

A FTIR spectrometer is usually composed by the following key components:

- A broadband IR source that emits all the recorded wavelengths simultaneously
- A beam splitter that separates the IR beam into two equal parts
- Some mirrors necessary to define the length of the travel of the beam
- A reference laser source used to track the position of the mirrors
- Some focusing optics used to transfer the beam into the sample cell and then from it to the detector
- A sample cell filled with sample gas or test gas
- An IR detector which responds to the entire wavelength range of the spectrometer
- A laser detector which responds to the wavelength of the reference laser

The beam splitter and the group of mirrors are known as the interferometer, which can be considered an optical modulator. The modulation of the beam is fundamental to calculate the intensity at each frequency from the signal recorded by the IR detector. The IR detector records a signal as a function of time known as the interferogram. This signal is linked with the IR spectrum by a Fourier transformation. By placing a sample cell between the interferometer and the detector, the spectrometer can be used to measure the absorption spectrum of the sample gas. From it, it is possible to calculate the concentration of gases in the sample. A schematization of the components of the FTIR is shown in Figure 10.

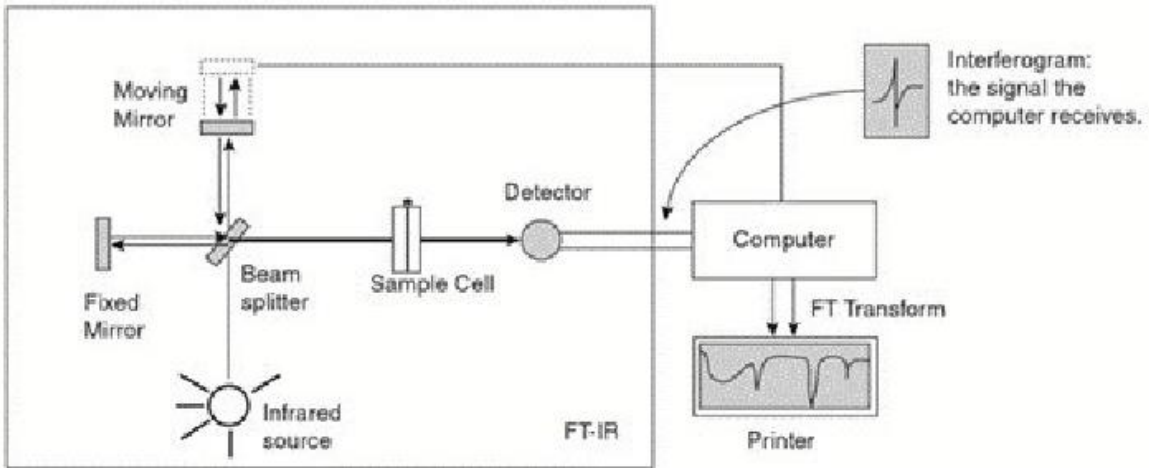


*Figure 10 - FTIR schematization [15].*

### 1.3.2 Tunable Diode Laser (TDLAS)

Tunable Diode Laser Absorption Spectroscopy (TDLAS) is a trace gas sensing technique that can be employed in many fields, such as industrial process monitoring and control, environmental sensing or plant safety. TDLAS sensors can offer high sensitivity, specificity, fast response, ease of calibration and operation, ruggedness and portability [16]. Moreover, it is a contactless equipment, because only the laser beam has to interact with the sample. Thanks to these potentialities, leak detection of methane using TDLAS approach is becoming a popular method.

The beam is generated using a semiconductor material that emits light when current passes into the semiconductor junction.

The gas concentration is detected measuring the amount of laser light that is absorbed when the beam passes through a sample of gas. The absorption spectra are recorded and then combined with other quantities such as the effective path length, the temperature and the pressure to determine the effective concentration of the desired gas [17].

Exactly as the FTIR, also TDLAS technique is based on the Lambert-Beer law.

Thanks to the fact that the wavelength emitted is narrow and can be chosen for a specific compound (each molecule absorb energy at a specific wavelength), interferences are usually absent. In fact, at wavelengths different to the chosen one there is essentially no absorption.

A schematization of a TDLAS is shown in Figure 11. it is possible to observe that the laser has a fixed length that is set thanks to the use of mirrors.

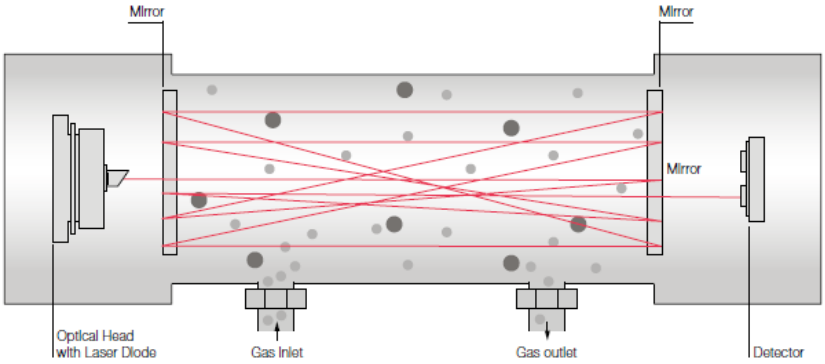


*Figure 11 - TDLAS schematization [18].*

### 1.3.3 Other techniques

To detect the emissions of $CH_4$ it is also possible to use optical gas imaging (OGI) systems. The most common technology relies on infrared imaging. Usually, IR camera creates images of a narrow range of the IR spectrum, between 3.3 and 3.4 um [19].

The radiant energy incident on the sensor of the infrared camera is measured. This energy essentially can come from four sources: from the plume, from the background, from the sky (usually one order of

magnitude lower than the others and so negligible) and from the atmosphere (negligible at short distances). All these radiances are function of the temperature and of the emissivity of the body. The background emissivity is assumed constant and the pixel of the camera registers an intensity change if the value of the radiance is bigger than the Noise Equivalent Power (NEP) of the IR camera. This value depends on the mechanical characteristics of the camera. This approach is often adopted in the oil and gas industry, but it could be implemented also in other environmental sectors, such as in the detection of leaks from a biogas plant [20].

# 2 Methane emissions in an anaerobic digestion plant

Biogas plants produce energy thanks to the anaerobic digestion of organic sources such as livestock manure, organic fraction of municipal solid waste, waste from food industry, energy crops, and mixtures of the aforementioned feedstocks.

Europe is the largest producer of biogas worldwide [21], with Germany being the largest contributor, and countries like Denmark, France, Italy and Netherland actively promoting the production of biogas, as well. According to the Statistical report of the European biogas association 2020, there are about 19,000 biogas plants (dedicated to electricity production) and 725 biomethane facilities spread over the European territory, which produced 167 TWh of electricity and 26 TWh (about 2.7 bcm) of biomethane, respectively [20].

Biogas and biomethane production plants are deemed as virtually zero emissions as the biogas combustion in these plants (or the biomethane combustion) is the last step of a process that started from $CO_2$ capture from the atmosphere by vegetation and, in addition, the controlled anaerobic digestion replaces the aerobic degradation that would result in the production of $CO_2$. It is therefore clear that the emissions of $CH_4$ from these plants reduce the net GHG benefits, so it is necessary to develop reliable methods to quantify the effective losses of GHGs. In the last few years, this field is developing a lot and two main approaches have been identified: on-site method and off-site method [13].

On-site approach is generally used to identify and quantify single emissions from hotspots. They can be for example related to the storage of the digestate or to leaks from biogas-bearing plant components.

Off-site approaches are necessary to estimate the whole-plant emissions of methane. The concentration of $CH_4$ in the surrounding area is measured and then, thanks to inverse dispersion modelling or tracer gas dispersion methods the results are obtained. These approaches are able to monitor time-variant and operational emissions over a long period, but they depend on atmospheric dispersion, weather conditions and topography of the area.

## 2.1 Description of the site

The site is located in the south of Piedmont, in the province of Cuneo. Figure 12 is an aerial view of the site. The main components are:

- Stall (blue circle)
- Sewage storage (yellow circle)
- Digestate storage (red circle)
- Manure storage (orange circle)
- Biogas plant (green circle)

Test have been conducted on December 23rd 2022.

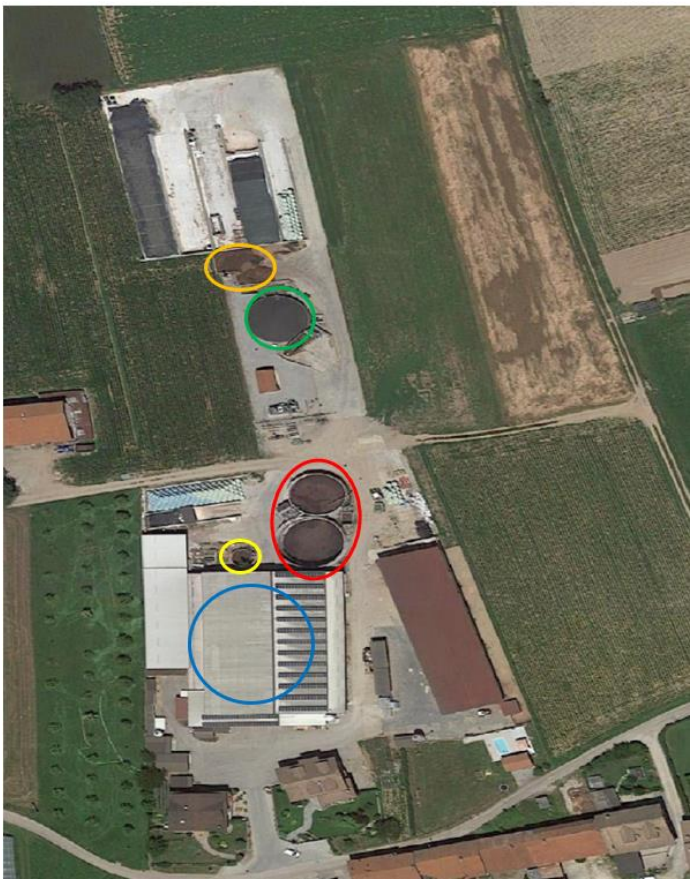

*Figure 12 - Biogas plant.*

## 2.2 Measurement methodology

### 2.2.1 Meteorological data

Meteorological data have been obtained through a weather station produced by OneConcept. It has been placed at 150 m from the plant at a height of 1.5 m. It can be observed in Figure 14. It is able to record wind direction and speed with a precision of ±1 m/s when wind velocity is lower than 10 m/s. Recording time of the measures has been set to 5 minutes.

To get more data, wind speed and direction of two other weather stations present on the website "Weather Underground" [22] have been downloaded (named IBOVES15 and IBOVES16). Their location is shown in Figure 13.

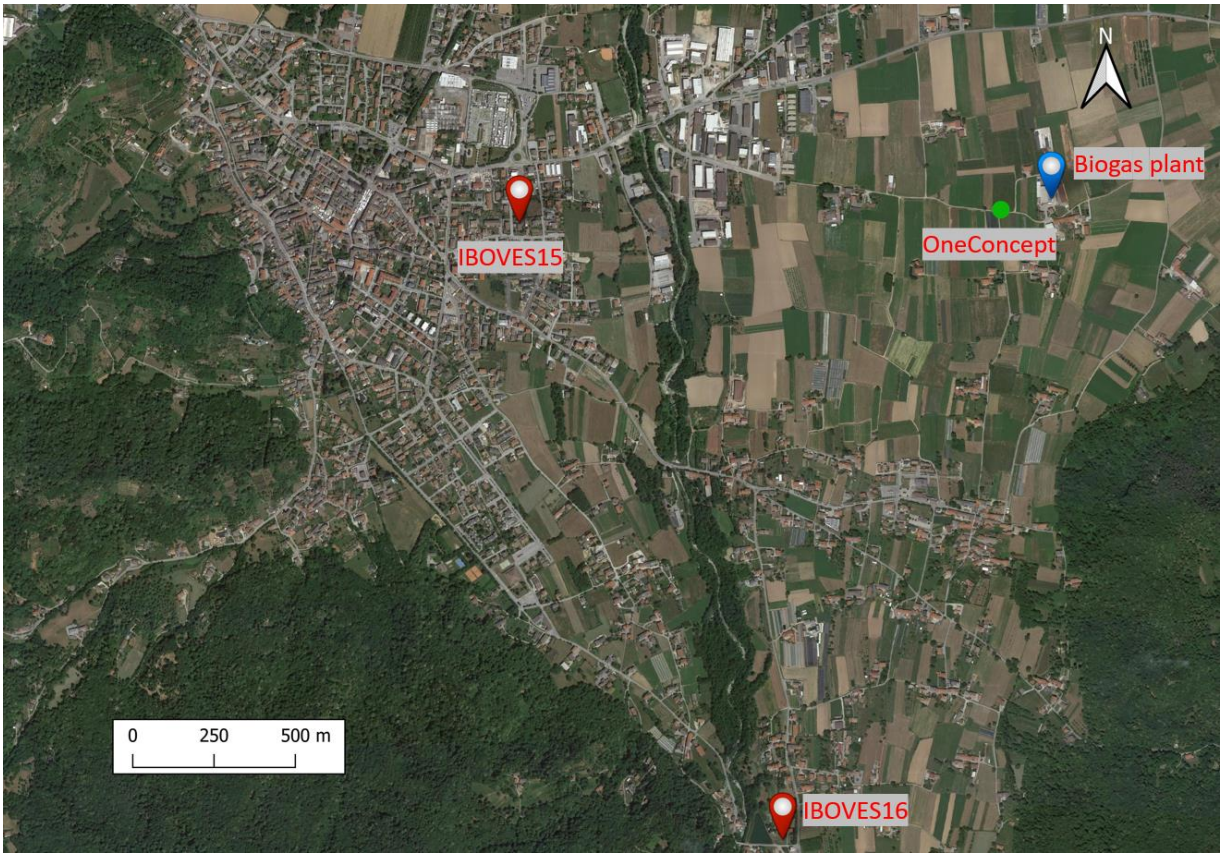


*Figure 13 - Position of the weather stations.*

*Figure 14 - OneConcept weather station.*

The variation of the wind speed can be seen in Figure 15, while the variation of the wind direction is reported in Figure 16.

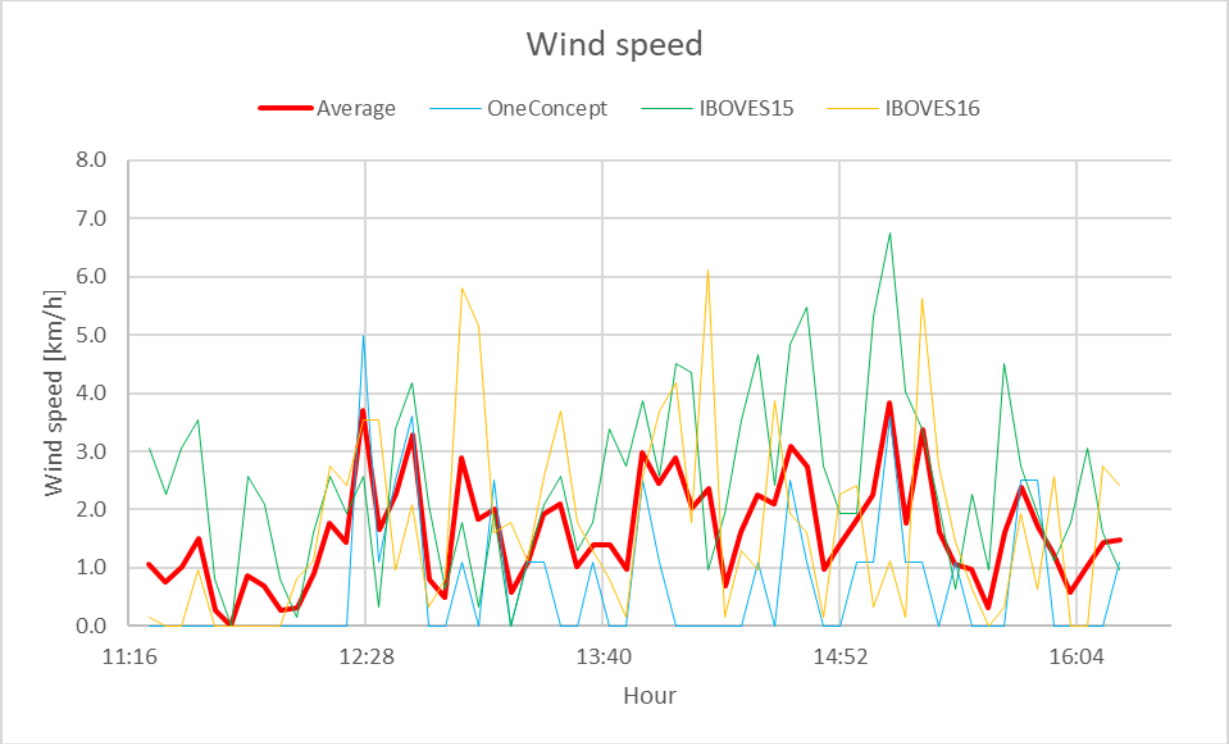


*Figure 15 - Wind speed variation during the day.*

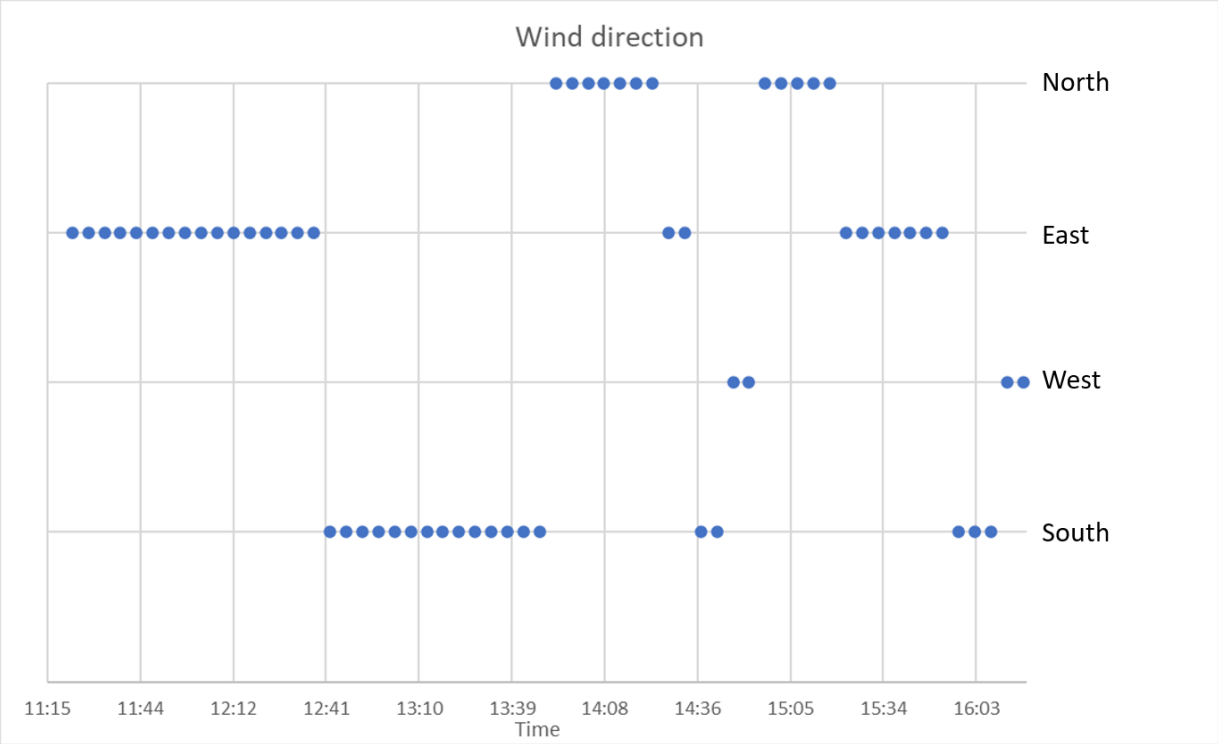


*Figure 16 - Variation of the wind direction during the day.*

### 2.2.2 FTIR

An ETG FTIR 9500 device, produced by the company ETG Risorse e Tecnologia s.r.l., was used. The temperature of the cell was set at 45 °C and the path of the beam is 5 meters. Spectra are recorded in a range between 833 and 4999 $cm^{-1}$. The sampling rate is 1 Hz, but the instruments provide only one measure every 90 seconds because it averages all the spectra to reduce to the minimum the noises.
Data can be observed remotely using a tablet.
The power supply was guaranteed by a battery of 80 Ah connected to an inverter.
Figure 18 shows the main page that can be seen from the monitor, where the values of each gas are shown in real time. The configuration adopted can be changed, adding all the compounds that are considered necessarily. In the case of this thesis, the two main gases that has been measured were $CO_2$ and $CH_4$. During the sampling time it is also possible to observe the spectrum (Figure 19) and the absorbance (Figure 20). The background process has not been performed the days before the measures for logistic problems, and from the spectrum it is possible to observe that it is not aligned with the FTIR measurements. However, given that the graphs related to the absorbance present good results, the background issue can be considered negligible and does not affect the overall results obtained from the instrument.

*Figure 17 – ETG FTIR 9500.*


*Figure 18 - Main page of the FTIR.*

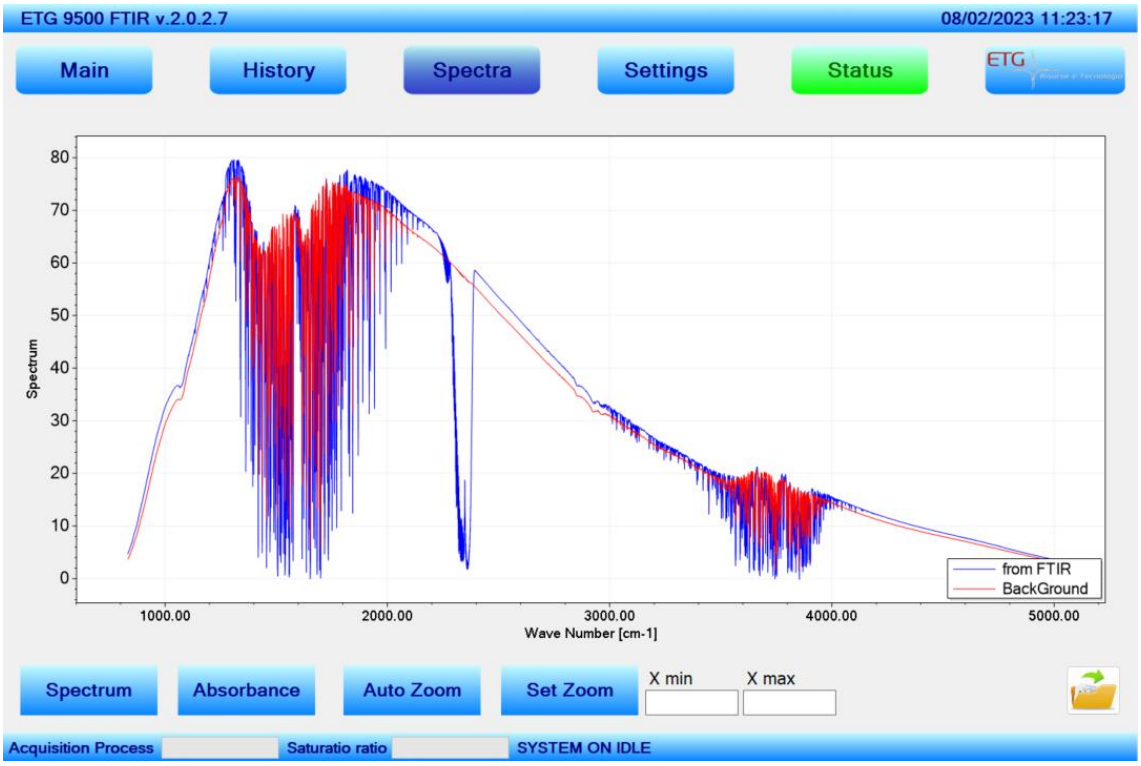


*Figure 19 - Spectrum of a measurement averaged over a 90 second period.*

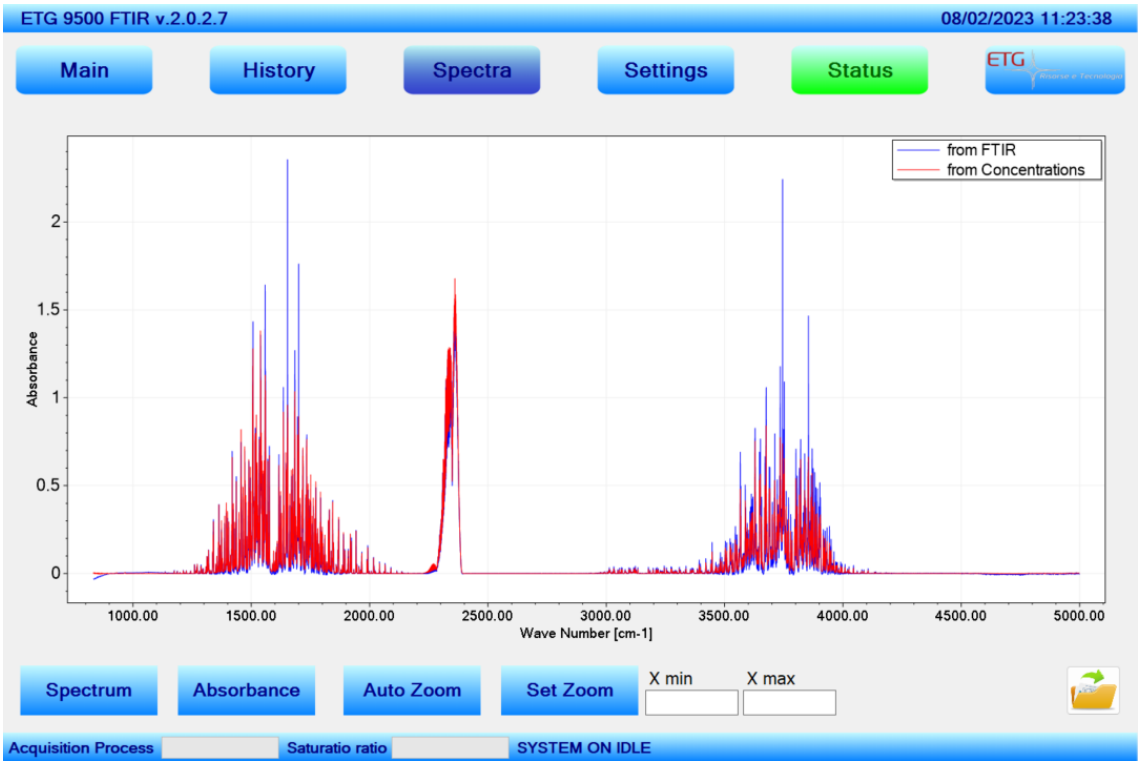


*Figure 20 - Absorbance of a measurement averaged over a 90 second period.*

### 2.2.3 TDLAS

The TDLAS used during this measurement campaign was the LGD compact A produced by Axetris. Characteristics are reported in the Table 13. From Figure 21 it is possible to see the small dimensions of the instrument. Thanks to the ease of movement, it has been fundamental to make surveys throughout the site. Using the app "VNC Viewer", it has been possible to see in real time the concentration of methane. This tool proved very useful to understand in real time the presence of GHG hotspots.

*Table 13 - LGD compact A characteristics.*

| | | |
|---|---|---|
| **Measuring range** | ppm | From 0 to 100 |
| **Resolution** | ppm | 0.01 |
| **Sampling rate** | Hz | 2 |
| **Operating temperature range** | °C | From -10 to 50 |

*Figure 21 - TDLAS portability.*

### 2.2.4 Positioning

Two GPS systems have been used. The position of the FTIR has been obtained thanks to a Amazfit Bip S smartwatch, while the position of the TDLAS has been recorded by a Polar M430 watch. In both cases, the positioning precision is in the order of 2 m, but it has been considered acceptable because of the dimension of the site that has been analysed. Data have been then imported on the software QGIS. Starting from the total points provided by the GPS, 39 of them have been chosen as representative points and their position is shown in Figure 22. Points from 40 to 46 have been inserted during the post processing analysis to obtain a more realistic model. Their values of concentration have been considered equal to the one corresponding to the point 39.

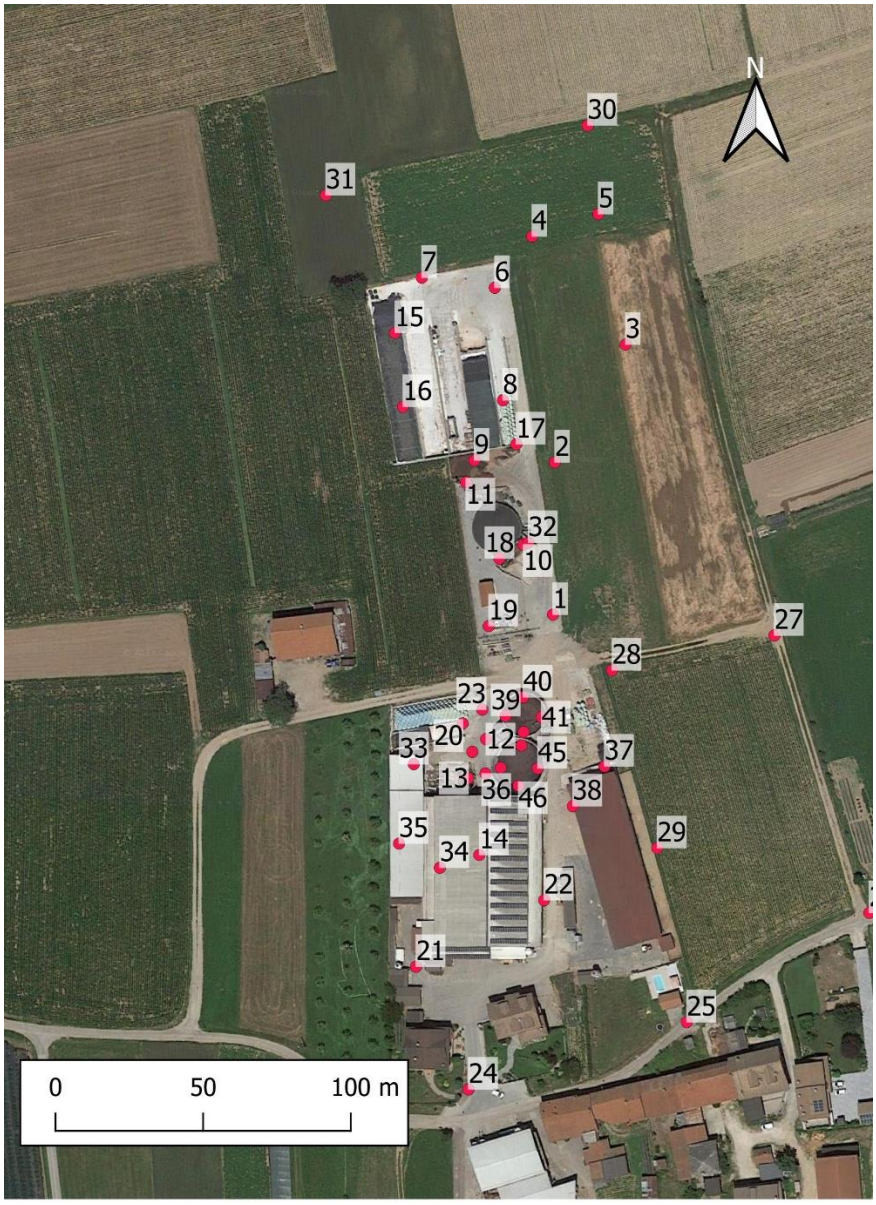


*Figure 22 - Selection of measurement points.*

## 2.3 Results and discussion

Because of their different sampling rate (FTIR provides a value over a period of 90 seconds, TDLAS provides 120 measurements per minute), FTIR has been placed for longer period in specific places (from few minutes to 50 minutes, depending on the stability of the values observed), while the TDLAS has been used to cover the entire area of the site of interest.

Thanks to this methodology, it has been possible to set a value of methane in the close environment and to detect the main hotspots for methane emissions.

### 2.3.1 Mapping of $CH_4$ concentrations

The first aspect to consider during the measurement of methane emissions was the comparison between FTIR and TDLAS. For this reason, some points have been recorded by both the instruments. The results are shown in the Table 14 and in Figure 23. For the table, also the standard deviation (σ) of the points has been considered.

*Table 14 - FTIR and TDLAS measurement comparison. Concentrations in ppm.*

| Point | FTIR average | FTIR σ | TDLAS average | TDLAS σ |
|---|---|---|---|---|
| 2 | 2.69 | 0.63 | 1.95 | 0.01 |
| 5 | 2.49 | 0.50 | 1.91 | 0.02 |
| 6 | 1.76 | 0.63 | 2.12 | 0.11 |
| 7 | 1.96 | 0.53 | 2.19 | 0.06 |
| 8 | 2.19 | 0.77 | 2.34 | 0.18 |
| 9 | 2.85 | 0.84 | 2.58 | 0.63 |
| 10 | 2.48 | 0.71 | 2.60 | 0.72 |
| 11 | 2.87 | 1.84 | 2.16 | 0.03 |
| 12 | 3.61 | 2.37 | 5.55 | 1.60 |
| 13 | 9.93 | 4.43 | 10.21 | 3.25 |
| 14 | 16.92 | 2.82 | 24.86 | 5.23 |

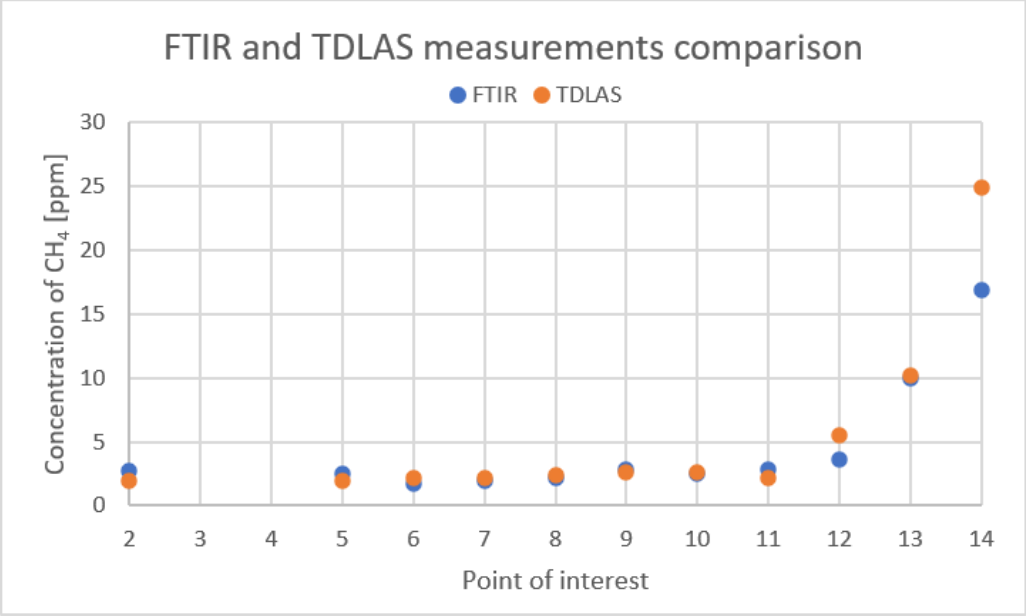


*Figure 23 - FTIR and TDLAS measurement comparison*

Regarding the behaviour of the FTIR, the highest values of standard deviation have been reported in the areas where methane concentration was higher. In particular:

- For point 12, the standard deviation has been affected by the fact that the FTIR has been placed at different distances (from 5 meters to 1 meter) from a pile of manure and because of the gusts of wind. Also point 13 suffered variations because of the wind.
- Point 14 is the one that corresponds to the barn. Values have been affected by the presence of animals and by the workers that were performing their job. The difference of 8 ppm between the average concentrations of TDLAS and FTIR can be explained by the fact that with TDLAS the centre of the stall has been reached. Figure 24 shows how the methane concentration progressively increased getting close to the centre.

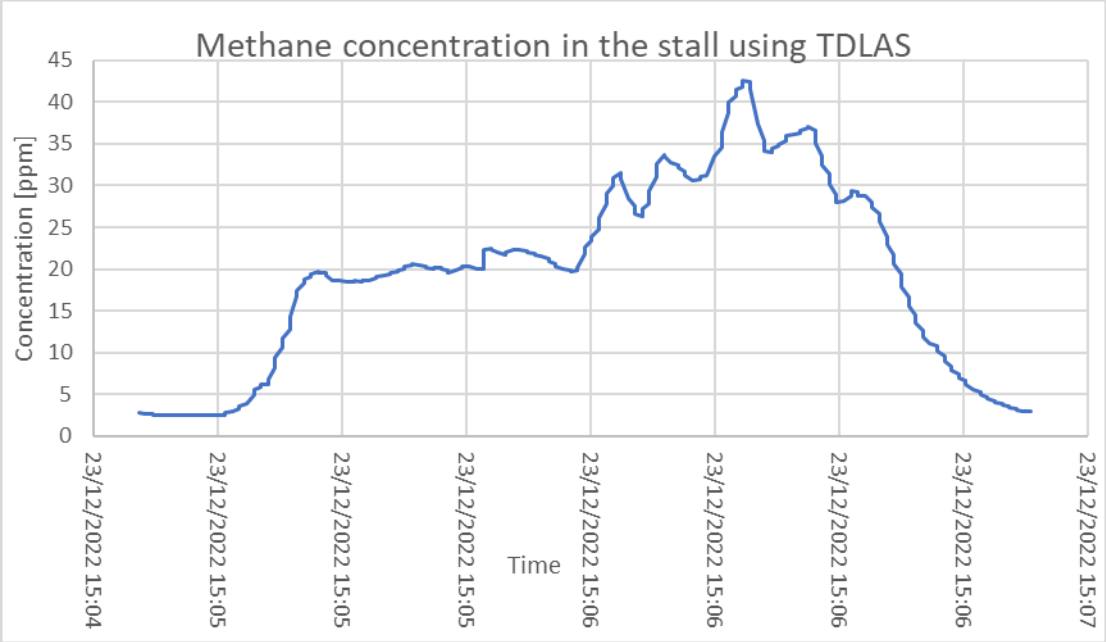


*Figure 24 - Methane concentration in the stall using TDLAS.*

In conclusion, in all the points in common the concentrations recorded by FTIR and TDLAS were considered comparable. For this reason, covering the whole site with only the TDLAS has been considered a good solution.

Point 11 corresponds to the storage of fresh manure. The high value of σ is a consequence of the manure handling. During the measurements (for this point the FTIR recorded 25 minutes of data), an operator brought fresh manure, causing an increase in the concentration of $CH_4$, as clearly visible from Figure 25. This example demonstrates that the variability of the concentrations is strongly dependent on the boundary conditions and that the results are therefore affected by uncertainties.

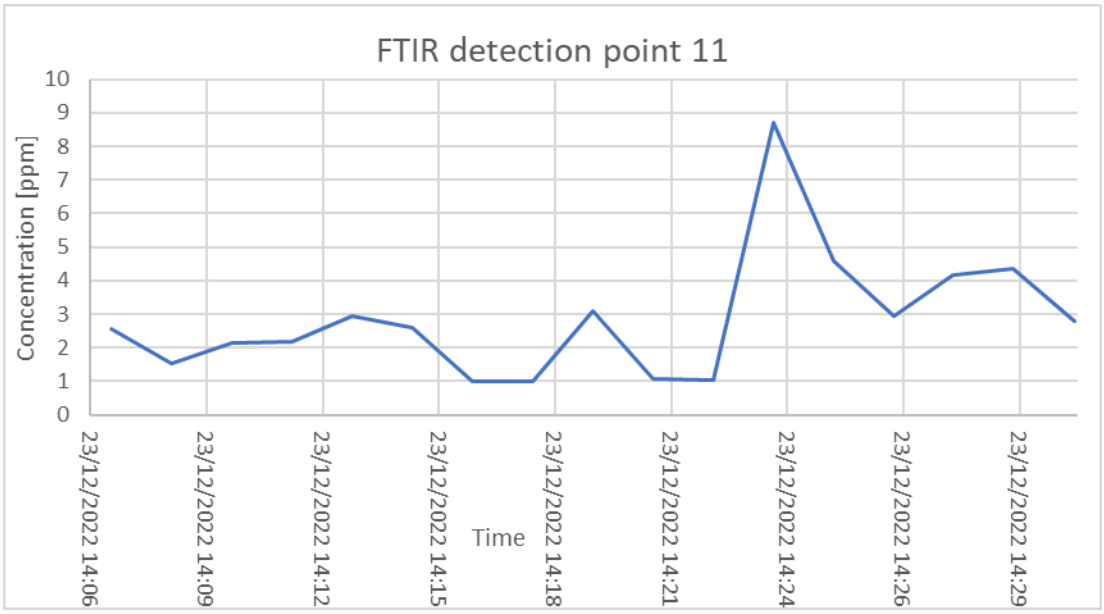


*Figure 25 - Peak caused by the handling of the manure.*

Another example related to the variability of measurements can be found in the point 23. Its location is between the sewage storage and the digestate storage. Figure 26 shows some peaks. Looking at the meteorological data, it is possible to hypothesize that this behaviour is due to the sudden variation of the wind direction, which changed for a short time from North to West. For this reason, the point remained downwind the digestate storage, which is the biggest hotspot of this site, for a short time.

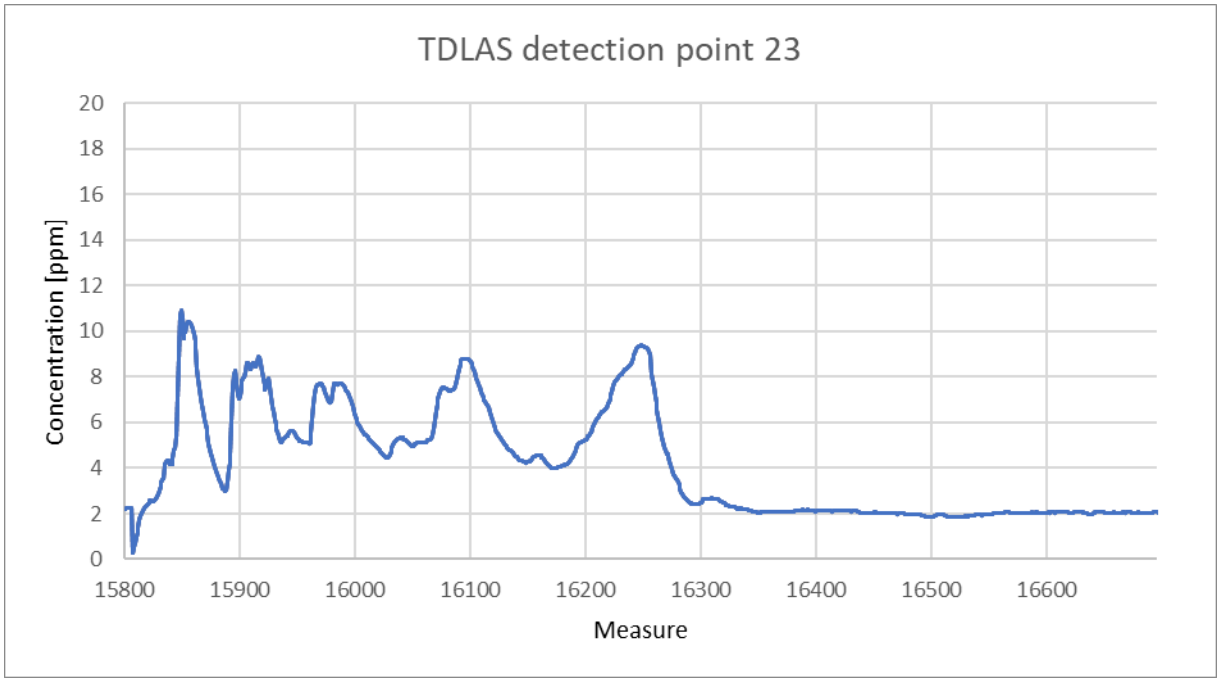


*Figure 26 - Peak caused by a gust of wind.*

The methane concentrations at all selected points are summarized in the Table 15.

*Table 15 - Methane concentrations of the points in ppm.*

| Point | Concentration | Point | Concentration | Point | Concentration |
|---|---|---|---|---|---|
| 1 | 4.96 | 14 | 20.89 | 27 | 2.00 |
| 2 | 2.32 | 15 | 2.14 | 28 | 1.99 |
| 3 | 2.85 | 16 | 2.12 | 29 | 1.96 |
| 4 | 2.29 | 17 | 2.25 | 30 | 1.85 |
| 5 | 2.20 | 18 | 2.13 | 31 | 1.90 |
| 6 | 1.94 | 19 | 2.09 | 32 | 2.41 |
| 7 | 2.07 | 20 | 5.85 | 33 | 4.40 |
| 8 | 2.27 | 21 | 2.29 | 34 | 11.36 |
| 9 | 2.72 | 22 | 6.74 | 35 | 10.66 |
| 10 | 2.54 | 23 | 4.16 | 36 | 6.17 |
| 11 | 2.51 | 24 | 2.01 | 37 | 2.32 |
| 12 | 4.58 | 25 | 2.01 | 38 | 2.22 |
| 13 | 10.07 | 26 | 1.98 | 39 | 82.73 |

As already anticipated, the highest concentration recorded during the day has been in correspondence to the digestate storage. In particular, the highest concentration obtained come from measurement performed on the top of the tank. The precise amount of digestate is unknown, but it was about one meter lower than the height of the wall (4 meters) present in Figure 27.

*Figure 27 - Digestate storage.*

As shown in Figure 28, concentration was unstable, probably because $CH_4$ concentration was higher than the range of measurements of the TDLAS. Unfortunately, it has not been possible perform a survey with the FTIR because of the prohibitive position of the location.

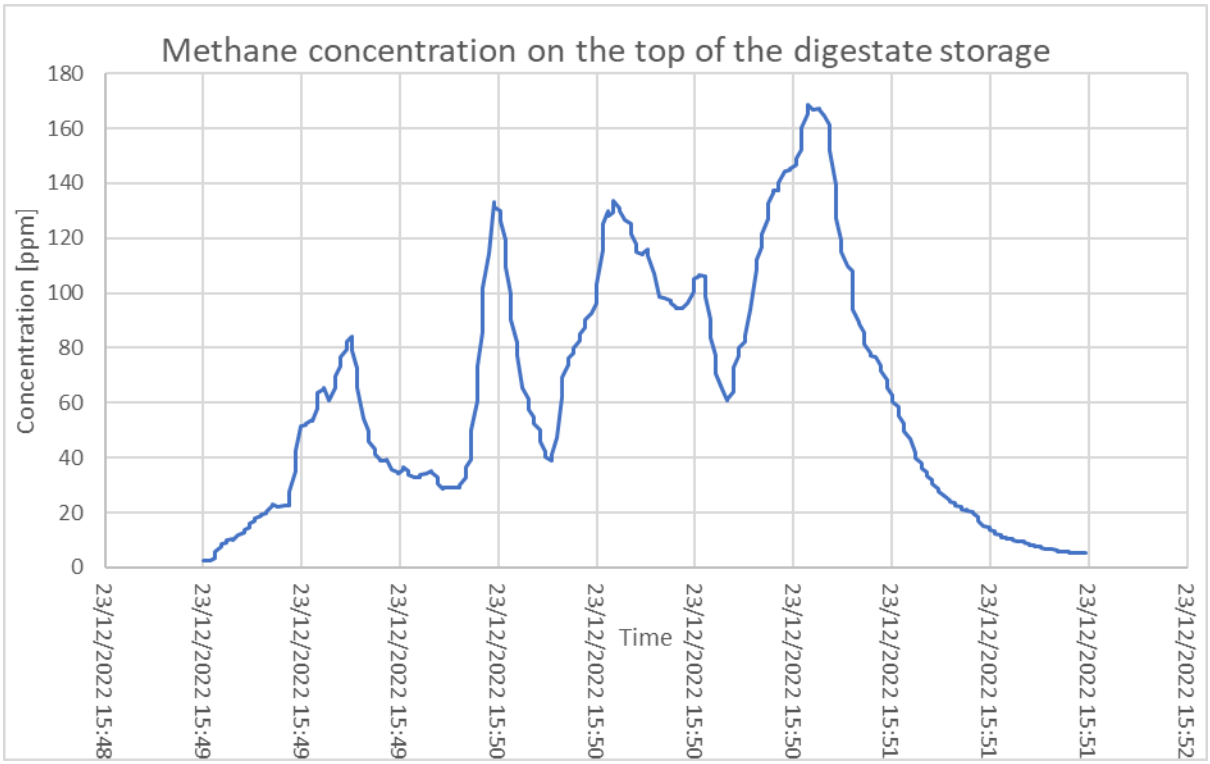


*Figure 28 - Methane concentration on the top of the digestate storage with TDLAS.*

Once obtained the concentration of each point, a model has been created thanks to the software Surfer. The interpolation of the points has been obtained using Kriging. The result can be seen in Figure 29.

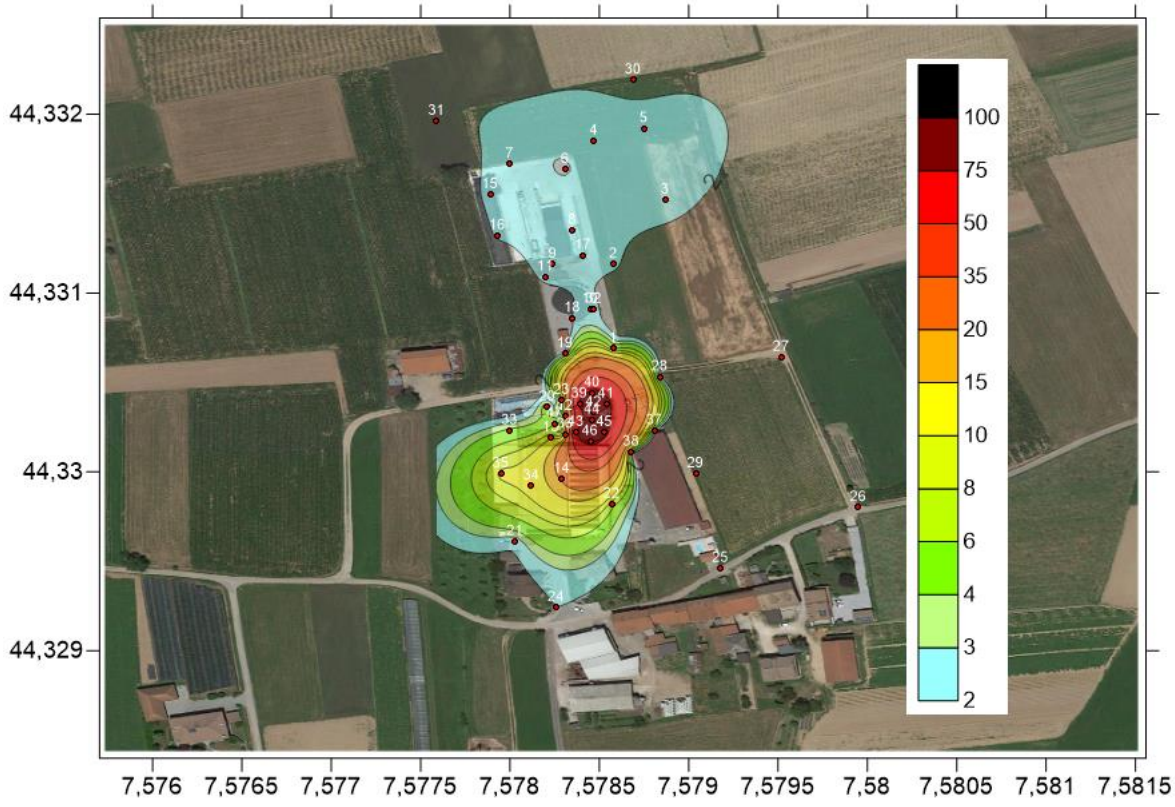


*Figure 29 - $CH_4$ concentrations in the biogas plant.*

From the model, it is possible to make some considerations. The main hotspot represented by the digestate storage is evident, but its influence covers a range only of 30-40 meters. The presence of the stall produces a protuberance of the plume in the south-west part of the site, while the fresh manure and the biogas plant don't affect in a massive way the surrounding areas. Moreover, the concentration in the cultivated fields is comparable to the background one.

### 2.3.2 Estimation of CH4 flux with gaussian plume inverse modelling

Both TDLAS and FTIR are not able to provide information about the flux. For this reason, an attempt has been made to reconstruct the flux using a gaussian plume model. To do that, it has been necessary to identify some points as hotspots, some points as receiver and to define some parameters.

Regarding the sources of emissions, the following points have been chosen: the one regarding the sewage storage (point 13), the stall (point 14), and the digestate storage (from point 39 to 46). Receivers have been identified in points 1, 19 and 28. They have been chosen because of their distance from the sources (between 50 and 80 meters) and because there were not obstacles between them and the sources.

Wind speed and direction have been obtained thanks to the meteorological station. In particular, the wind speed was 0.58 m/s and the wind direction was NNE.

The parameters needed to calculate the vertical and horizontal dispersion coefficient were derived using Pasquill stability classes. In this case, the stability class was B, because average surface wind speed was lower than 2 m/s and because the insolation was moderate. The formulas that have been used are:

$$\sigma_y = a * x * (1 + b * x)^c$$

*Equation 2*

$$\sigma_z = a * x$$

*Equation 3*

$\sigma_y$ and $\sigma_z$ are respectively the horizontal and vertical dispersion coefficient. a, b and c are the coefficients, resumed in Table 16, that must be defined from the Pasquill Stability Classes. x is the distance between the hotspot and the source considering the wind direction.

*Table 16 - Coefficients from Pasquill Stability Class B.*

| Coefficient | $\sigma_y$ | $\sigma_z$ |
|---|---|---|
| a | 0.16 | 0.12 |
| b | 0.0001 | 0 |
| c | -0.5 | 1 |

As said before, to calculate the flux of the site it has been used a Gaussian plume model. Given that the concentration of the receivers has been measured at ground level, the following formula has been used:

$$C(x, y, 0) = \frac{Q}{\pi * u * \sigma_y * \sigma_z} * \exp\left(-\frac{h^2}{2 * \sigma_z^2}\right)$$

*Equation 4*

Q is the source strength [mg/s], C is the concentration at the receiver [mg/m$^3$], u is the wind speed [m/s] and h is the height of release of the source [m].

Instruments provide the value of the concentration in ppm. To convert it into mg/m$^3$, it is necessary to perform the following calculation:

$$C\left[\frac{mg}{m^3}\right] = \frac{ppm * PM}{24.45}$$

*Equation 5*

Some assumptions were necessaries. The background concentration has been calculated averaging the values of the points from 24 to 31. The obtained result has been 1.96 ppm, which corresponds to 1.28 mg/m$^3$. Looking at the wind direction given from the OneConcept weather station, the angle of the wind direction has been set to 22.5°, that corresponds to a NNE wind direction. Its velocity has been set at 0.58 m/s.

To obtain the source of emissions of the selected points, a trial-and-error approach has been adopted. For each point, the process has been the following:

1. Calculation of the distance between source and receiver considering the wind direction.
2. Calculation of the average concentration in mg/m$^3$ of the receiver points from measurements
3. Arbitrary definition of the source strengths.
4. Sum of all the sources contributes (the result is summed to the background concentration).
5. Calculation of the square of the error between the results obtained from the model and from measurements.
6. Calculation of the average concentration in mg/m$^3$ of the receiver points from the model.
7. Calculation of the Root Mean Square Error (RMSE).
8. Comparison between the averages obtained from the model and the measurements.
9. Repetition of the process from point 3 until the RMSE is considered acceptable.

On Table 17 the results of the single points are reported, while Table 18 reports the overall results. Table 19 shows the source strength of all the hotspots. The highest concentration of point 1 respect the other two can be explained by the fact that the identified wind direction is almost parallel to the line of conjunction between the sources and the receiver.

*Table 17 - Concentrations from model and measurements of the single points.*

| Point | Model concentration [mg/m$^3$] | Measured concentration [mg/m$^3$] | Square error |
|---|---|---|---|
| 1 | 3.32 | 3.25 | 0.005 |
| 19 | 1.30 | 1.37 | 0.005 |
| 28 | 1.41 | 1.30 | 0.011 |

*Table 18 - Average concentrations from model and measurements.*

| Average concentration from the model [mg/m$^3$] | Average concentration from the measurements [mg/m$^3$] | RMSE |
|---|---|---|
| 2.01 | 1.97 | 0.083 |

*Table 19 - Source strengths.*

| Point | Source strength [mg/s] |
|---|---|
| 13 | 10 |
| 14 | 5 |
| From 39 to 46 | 40 |

Once concluded the trial-and-error approach, the source strengths have been summed to get the overall rate emission of $CH_4$ of the plant. The sum is equal to 335 mg/s, which means 10.565 $tCH_4$/year. Applying a GWP of 82, the yearly emission of the plant is 866.29 $tCO_{2eq}$.

Methane production of animals is strongly dependent on many factors, such as the climate and the diet [23], but in general it is possible to consider that a single caw during the year emits between 62 and 120 Kg of $CH_4$ [24]. Assuming that the number of caws was around 100, the order of magnitude of the obtained result is considered reliable.

It is important to underline that this approach presents many problems. The first one is related to the wind speed and direction: small changes in the speed and in the azimuth cause an important variation in the results. The second one is related to the rapidity of the reduction of the methane concentration even at 50 meters from the main hotspot. Moreover, the topography of the site has not been inserted into the model. This approach is recommended only in case it is not possible to use an instrument capable of calculating the flux, like a flux chamber.

### 2.3.3 Comparison between $CH_4$ and $CO_2$ concentrations

The only instrument able to also record concentrations of carbon dioxide was the FTIR.

A first comparison between the two GHGs can be provided from a graphical point of view. Concentrations can be seen in Figure 30. It is difficult to see a common pattern. In some cases, both $CO_2$ and $CH_4$ increases. In other cases, an increase in $CO_2$ does not correspond to an increase in $CH_4$. Moreover, there are circumstances in which both gases increase but with different intensity. The explanation of this behaviour can be found in the different circumstances of the measurements.

The first case in which only the concentration of $CO_2$ increases corresponds to a measurement performed on a snowy meadow. The second one corresponds to an area in which there were dry and old manure.

Relatively to the cases in which $CO_2$ concentration increase much more than $CH_4$, the measures were performed respectively in correspondence of the fresh manure and of sewage.

The two cases in which both $CH_4$ and $CO_2$ increase correspond respectively to the measurement at one meter from the solid digestate and the measurements preformed in the stall.

From this analysis, a possible explanation of the missed correspondence between the concentration of the two gases can be found in the different states of the manure: during its maturation, manure reduces emissions of methane with a rate faster than $CO_2$. The low correlation between the concentration of methane and carbon dioxide is confirmed by the scatter plot visible in Figure 31. The value of $R^2$ is 0.46, which confirm everything that has been said previously.

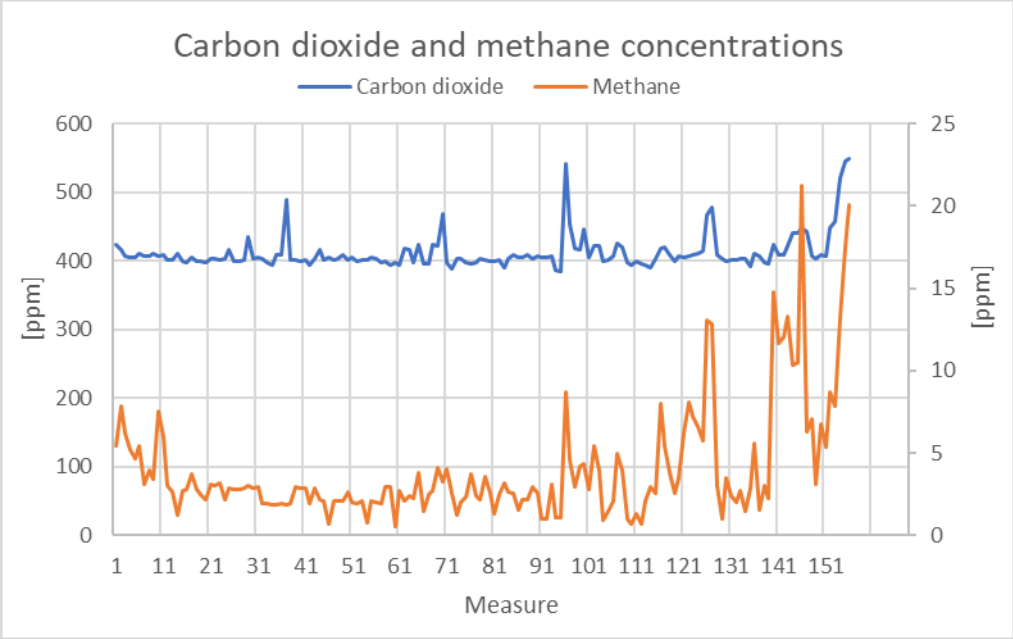


*Figure 30 - Carbon dioxide and methane concentrations comparison.*

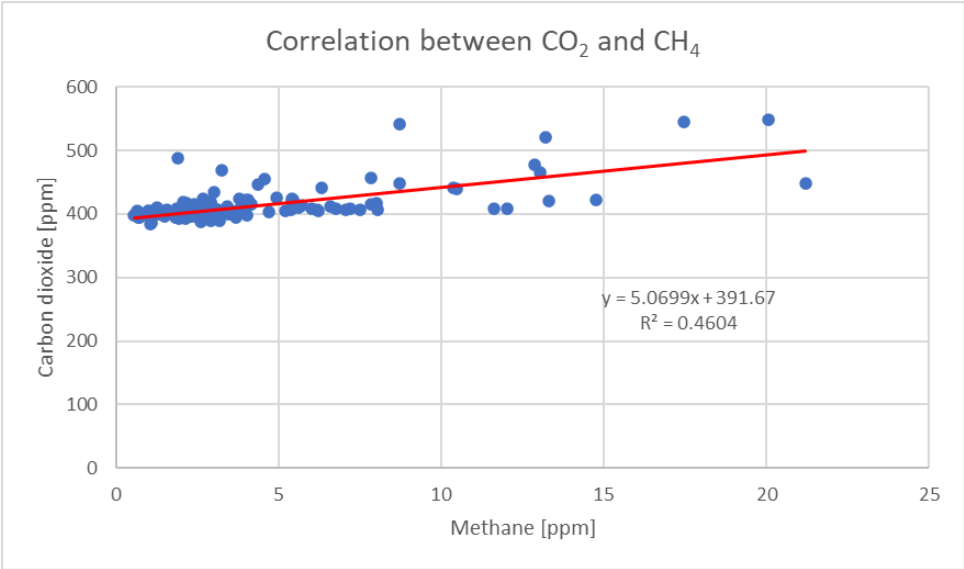


*Figure 31 - Correlation between carbon dioxide and methane concentrations.*

### 2.3.4 Other gases ($NH_3$)

Thanks to the configuration of the FTIR, during the day it has been possible to record the concentration of $NH_3$. The results are visible in Figure 32. It is possible to observe that the peak has been registered in correspondence of the sewage storage.

From the Legislative Decree 81/2008, the TLV – TWA (Threshold Limit Value – Time Weighted Average) must be lower than 25 ppm, so during the whole day the concentration remained always below this threshold. From an environmental point of view, the concentrations recorded do not justify a deeper investigation related to this gas.

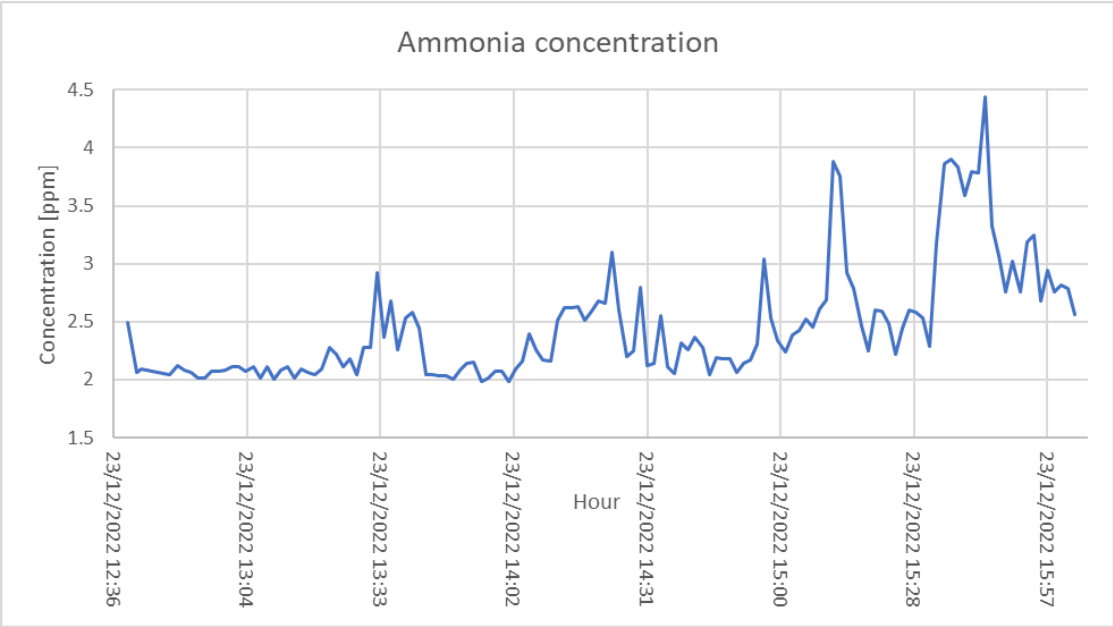


*Figure 32 - Concentration of $NH_3$.*

## 2.4 Lessons learnt and possible developments

In conclusion, the two instruments provided similar results when compared in the same points. For this reason, FTIR should be mainly used in some precise points of interest for at least 30 minutes, while TDLAS is the perfect instrument to cover the whole site in an efficient way.

Methane concentration decay very fast. Approximately, at 40 meters from the digestate tanks there were already values of concentration similar to the atmospheric ones. For this reason, all the approaches which require measurements far from the site (such as UAVs surveys or tracer detection methods) are not recommended.

To improve the results, a flux chamber could be used to understand the flux coming from the digestate storage, that can be considered the only one big hotspot. As said before, the model implemented to define the emission rate of the plant is not precise, providing reliable information only about the order of magnitude of emissions.

# 3 Methane emissions in a municipal solid waste landfill

GHG emissions from landfills are a widely acknowledged issue. For example, municipal solid waste (MSW) landfills are the third largest source of $CH_4$ emissions in the USA (14.5% of methane emissions in 2020 [25]) and the second largest in Europe (20% of emissions in 2016 [8]).

In 2018 in the USA about 50% of the 292 million tons of MSW generated have been sent to landfill. It has been calculated that on average 1 million tons of MSW produces around 8.5 $m^3$ per minute of LFG. Obviously, this data can be taken only as reference because it is strongly dependent on the composition of the organic matter and on the climate of the area where the landfill is placed [25].

Basing on other studies, in 2014 from the 123 Mt of MWS produced in USA, around 115.7 Mt of $CO_{2e}$ were produced [26].

If a time window of 30 years is considered, each tons of MSW could produce 200 $m^3$ of LFG [27].

The amount of degradable carbon in waste can be calculated multiplying the wet weight of waste with the degradable organic carbon (DOC) content. It must be considered that not all the carbon present converts to LFG. It is possible to assume that 50% of DOC in landfilled wastes can be converted into LFG [26].

LFG is a natural product of the decomposition of organic matter in anaerobic conditions.

The composition of the gas is usually made of 50-60% of $CH_4$ and 40-50% of $CO_2$. 2-5% is made of other compounds (non-methane organic compounds like sulphides and traces of inorganic compounds).

When municipal solid waste (WMS) goes to the landfill, there is a preliminary phase that usually lasts less than one year in which aerobic reactions appear. In this condition, only little methane is generated. After that, bacteria start to decompose wastes and generate methane.

In Figure 33 it is possible to observe the typical behaviour of the LFG composition after waste placement.

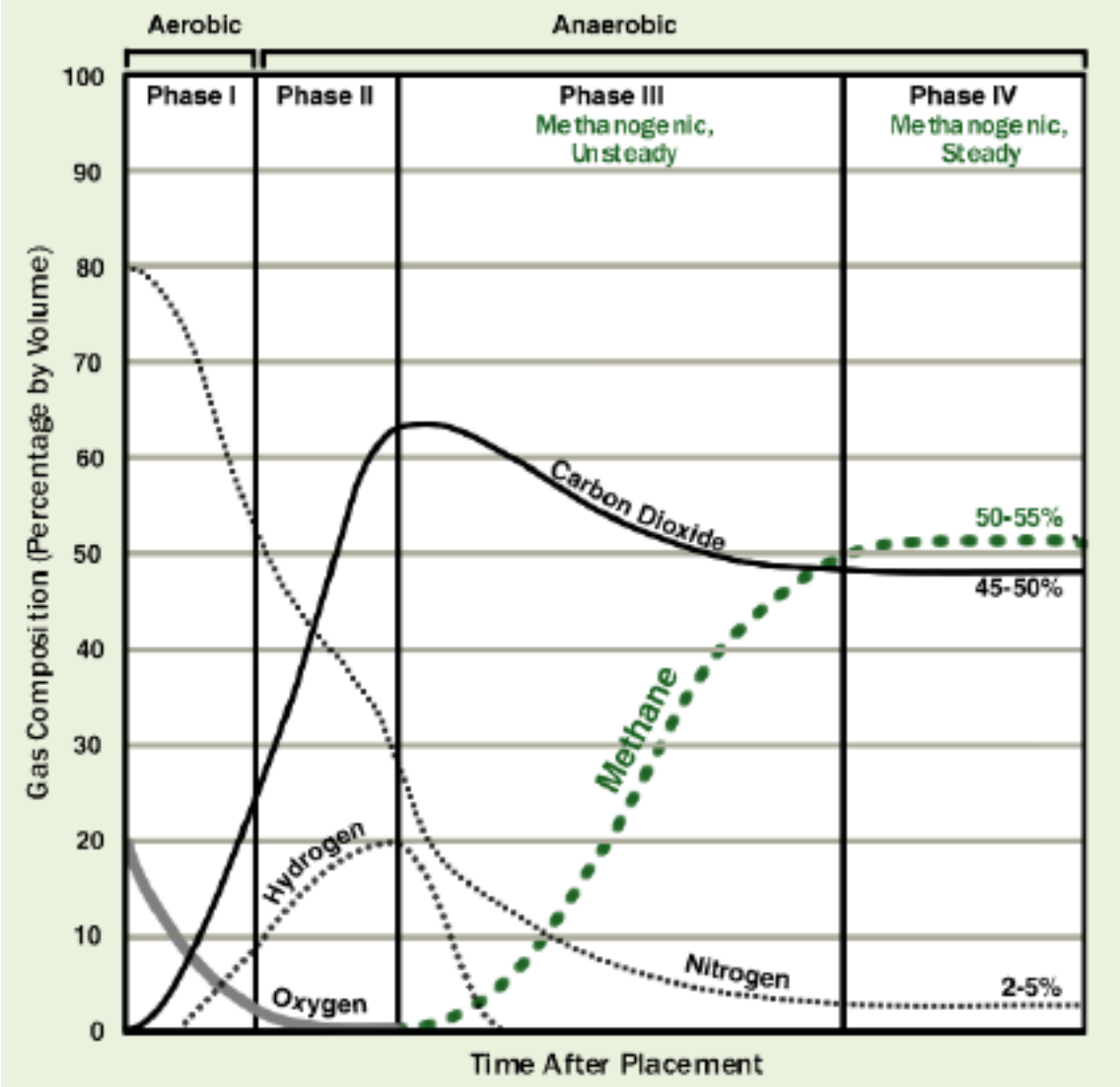


*Figure 33 - LFG composition depending on time [25].*

It can be observed that bacteria decompose wastes in four main phases. In each of this phase the composition of LFG changes. The total time needed and the duration of each phase strongly depends on the composition of the organic matter.

- Phase 1: aerobic bacteria break down the complex molecules (complex carbohydrates, lipids, proteins present in the organic wastes), producing mainly $CO_2$ and consuming oxygen.
- Phase 2: it starts when oxygen is exhausted. Anaerobic bacteria convert compounds created by aerobic bacteria into acetic, formic, and lactic acids and into alcohols such as ethanol and methanol. Carbon dioxide and hydrogen are produced.
- Phase 3: the organic acids produced in the previous phase are consumed by the anaerobic bacteria. During this process, the landfill becomes a more neutral environment in which methane-producing bacteria start to consume carbon dioxide and acetate.

- Phase 4: the composition and the production rate of LFG remain more or less constant. This phase can last for decades.

These four phases can be expressed through two main processes:

- Acetogenesis: $C_6H_{12}O_6 \rightarrow 2C_2H_5OH + 2CO_2$
- Methanogenesis: $CH_3COOH \rightarrow CH_4 + CO_2$; $CO_2 + 4H_2 \rightarrow CH_4 + 2H_2O$

The gas produced by the landfill is then used to produce energy, but fugitive emissions are important anthropogenic sources of GHGs (in particular methane). For this reason, monitoring the landfill with the identification of hotspots and plumes is an important tool to reduce emissions.

To identify the fugitive emissions of LFG three main factors must be considered:

- Meteorological conditions (precipitation, wind, pressure, temperature)
- Soil and cover conditions (presence of fissures, permeability, porosity, moisture content, organic content, diffusivity)
- Waste and landfill conditions (lateral migration area, gas vents, gas production rate, internal barriers)

The amount of $CH_4$ emissions from landfill is often estimated through theoretical gas generation models. Intergovernmental Panel on Climate Change recommended to use a first-order decay (FOD) model, which is the most used approach. This model assumes that the organic matter in wastes decays slowly over a few decades and that at the same time there is production of $CH_4$ and $CO_2$. If constant conditions are assumed, the rate of methane production depends only on the amount of carbon remaining in the wastes [28].

Lately, FOD gas generation models have been improved adding site-specific process-based emission model that consider the local conditions such as soil type, climate, and oxidation rates.

Apart from theoretical models, to assess $CH_4$ emissions it is fundamental to apply direct measurements techniques. Many approaches are currently available, but until now none of them has been defined as the international reference one.

One of the most important aspects to consider is related to the scale that can be adopted. From a spatial point of view, measurements are made from the landfill surface (high precision but low representation of the whole situation) to distances of some kilometres (evaluation of emissions of a large area, but sensitive to surrounding sources), while from a temporal point of view the timescale can vary from few minutes to months. Moreover, temporal and spatial variability of the LFG emissions must be taken into account. Temporal variability is caused by the change of the weather conditions, while spatial variability can be very huge ($CH_4$ emissions rate in a landfill could vary up to seven orders of magnitude [29]) and is caused by many factors, such as the presence of cracks or holes in the soil cover.

In general, landfill emissions measurements are divided into two categories:

- Surface emission factor techniques: they are based on the quantification of emissions from a part of the landfill. From these measurements an emission factor is obtained and then applied to the remaining areas of the landfill
- Mass emission techniques: they quantify the landfill emissions from a larger area (sometimes directly from the whole landfill)

## 3.1 Description of the site

The landfill is in Cerro Tanaro, in the province of Asti.

The surveys have been conducted on January 17$^{th}$ 2023.

Measurements have been focused mainly on two parts of the landfill, which are reported in Figure 34: the first one was the area were MSW are deposited (red circle), while the second one was a depleted lot (yellow circle).

*Figure 34 - MSW landfill composition.*

## 3.2 Measurement methodology

### 3.2.1 Meteorological data

The weather station present in the landfill was out of service and, for this reason, the only data available have been obtained from a weather station present on the site Weather Underground [22] and far 8.5 km from the site.

### 3.2.2 FTIR

Exactly as for the biogas plant, the instrument that has been used is a ETG FTIR 9500.

### 3.2.3 TDLAS

Also in this case, the instrument that has been used is the same of the previous campaign.

### 3.2.4 Positioning

As for the measurements at the biogas plant, a Polar M430 GNSS watch was used to record the position of the TDLAS.

Data have been then imported on the software QGIS. Starting from the total points provided by the GPS, 92 of them have been chosen as representative points. Their position is shown in Figure 35.


*Figure 35 - Points selection on QGIS.*

## 3.3 Results and discussions

During this campaign of measurements, thanks to its portability, the main instrument used has been the TDLAS. FTIR has only been used to analyse the concentration of methane in correspondence of a torch.

### 3.3.1 Mapping of $CH_4$ concentrations

Concentration of methane has been measured on all the site. The highest density of measurements has been conducted in the cultivated part of the landfill (one measure every ten meters). All data have been recorded at a height of 10 cm from the landfill. In some cases, as visible in Figure 36, the concentration has been taken also at a height of 3 meters above the ground level. As visible from the part in the red

circle, at 3 meters from the ground the methane concentration was close to the atmospheric values of methane.

Starting from the 92 points selected for the evaluation of $CH_4$ concentration, 5 of them have been deleted because of the high value of standard deviation. An example is provided in Figure 37.

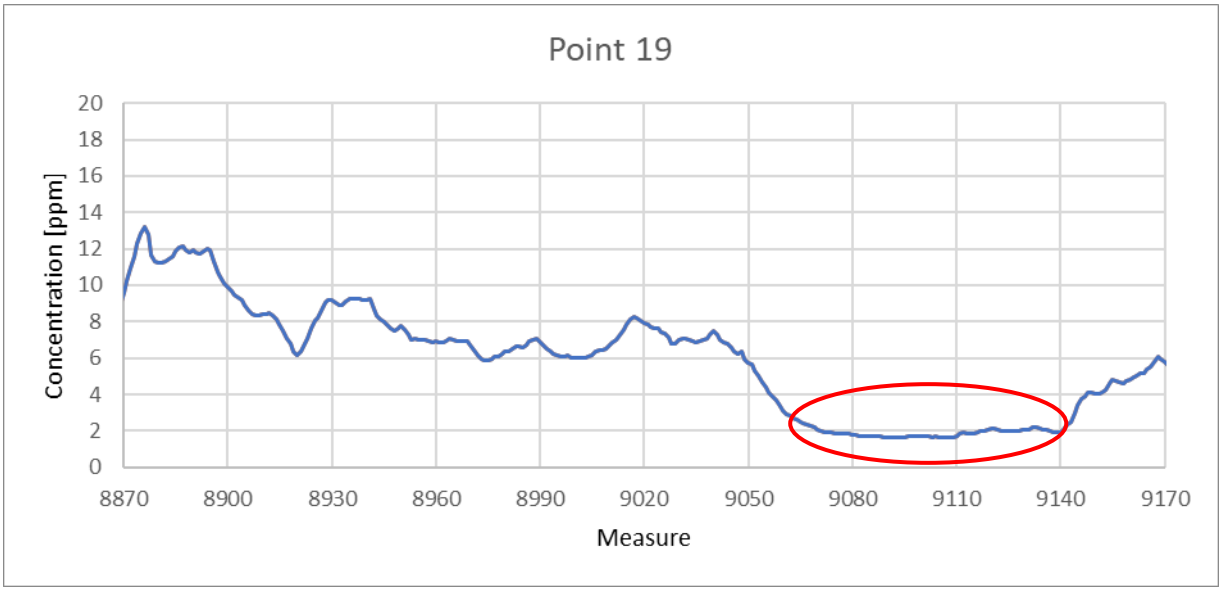


*Figure 36 - Methane concentration at 10 cm above ground level and 3 meters above ground level (red circle).*

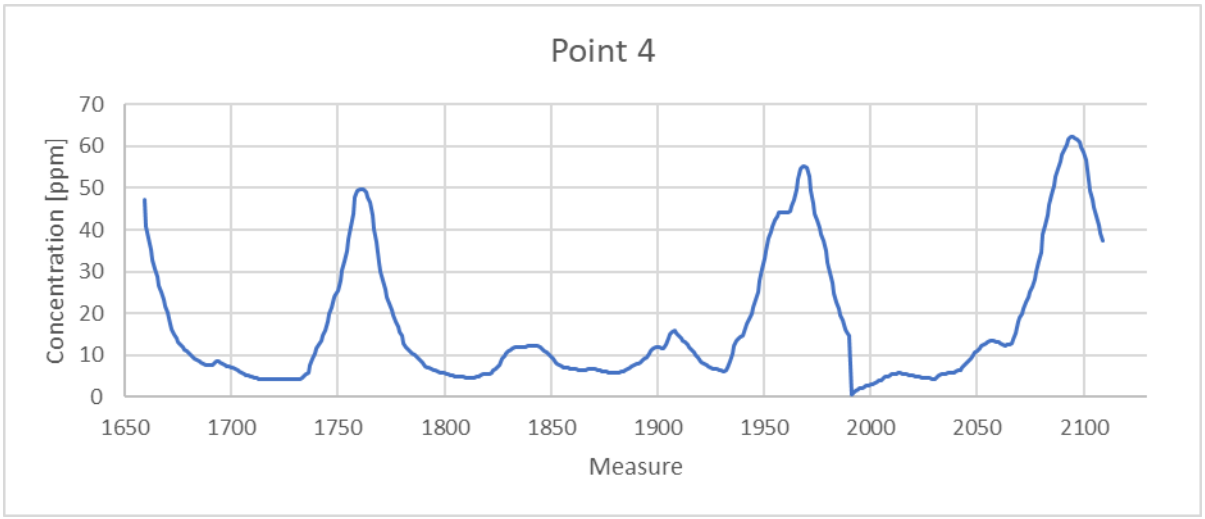


*Figure 37 - Variability of concentration on a single deleted point.*

All the concentrations of methane of the points are reported in Table 20.

*Table 20 - Methane concentration of all points.*

| Point | Concentration (ppm) | Point | Concentration (ppm) | Point | Concentration (ppm) |
|---|---|---|---|---|---|
| 1 | 2.26 | 32 | 5.23 | 63 | 15.20 |
| 2 | 2.20 | 33 | 5.53 | 64 | 64.53 |
| 3 | 39.70 | 34 | 3.87 | 65 | 407.24 |
| 4 | 16.88 | 35 | 3.43 | 66 | 12.03 |
| 5 | 2.51 | 36 | 2.51 | 67 | 5.82 |
| 6 | 4.52 | 37 | 2.46 | 68 | 14.33 |
| 7 | 9.79 | 38 | 2.27 | 69 | 2.07 |
| 8 | 4.66 | 39 | 3.89 | 70 | 2.00 |
| 9 | 7.69 | 40 | 3.34 | 71 | 2.07 |
| 10 | 9.12 | 41 | 3.34 | 72 | 2.41 |
| 11 | 4.30 | 42 | 7.50 | 73 | 3.23 |
| 12 | 4.74 | 43 | 12.00 | 74 | 3.42 |
| 13 | 3.07 | 44 | 59.26 | 75 | 2.30 |
| 14 | 3.22 | 45 | 40.39 | 76 | 15.48 |
| 15 | 15.47 | 46 | 36.72 | 77 | 16.75 |
| 16 | 7.82 | 47 | 84.55 | 78 | 12.29 |
| 17 | 2.62 | 48 | 5.27 | 79 | 6.10 |
| 18 | 407.24 | 49 | 5.11 | 80 | 5.46 |
| 19 | 5.93 | 50 | 11.98 | 81 | 9.75 |
| 20 | 15.53 | 51 | 11.40 | 82 | 6.45 |
| 21 | 3.42 | 52 | 6.93 | 83 | 5.90 |
| 22 | 59.42 | 53 | 20.64 | 84 | 5.88 |
| 23 | 7.39 | 54 | 9.41 | 85 | 6.09 |
| 24 | 1.58 | 55 | 7.41 | 86 | 1.94 |
| 25 | 1.72 | 56 | 11.28 | 87 | 1.86 |
| 26 | 1.75 | 57 | 6.84 | 88 | 1.88 |
| 27 | 1.71 | 58 | 13.28 | 89 | 5.25 |
| 28 | 1.70 | 59 | 25.77 | 90 | 5.84 |
| 29 | 2.04 | 60 | 34.05 | 91 | 7.06 |
| 30 | 7.59 | 61 | 7.99 | 92 | 6.54 |
| 31 | 5.50 | 62 | 407.24 | | |

As it can be observed from the results, the concentration of methane in the edges of the landfill is usually similar to the atmospheric one.

It must be highlighted that there have been some problems with the measurements of the concentration in correspondence to the torch. TDLAS has not been able to provide reliable data. For this reason, FTIR has been used to measure the concentration in correspondence of just one torch. The results obtained have been translated to the other torches. This is a strong assumption, because not all torches emit at the same rate and with the same concentration.

Moreover, neither the FTIR has been able to provide results that can be considered satisfying, as can be seen from Figure 38.

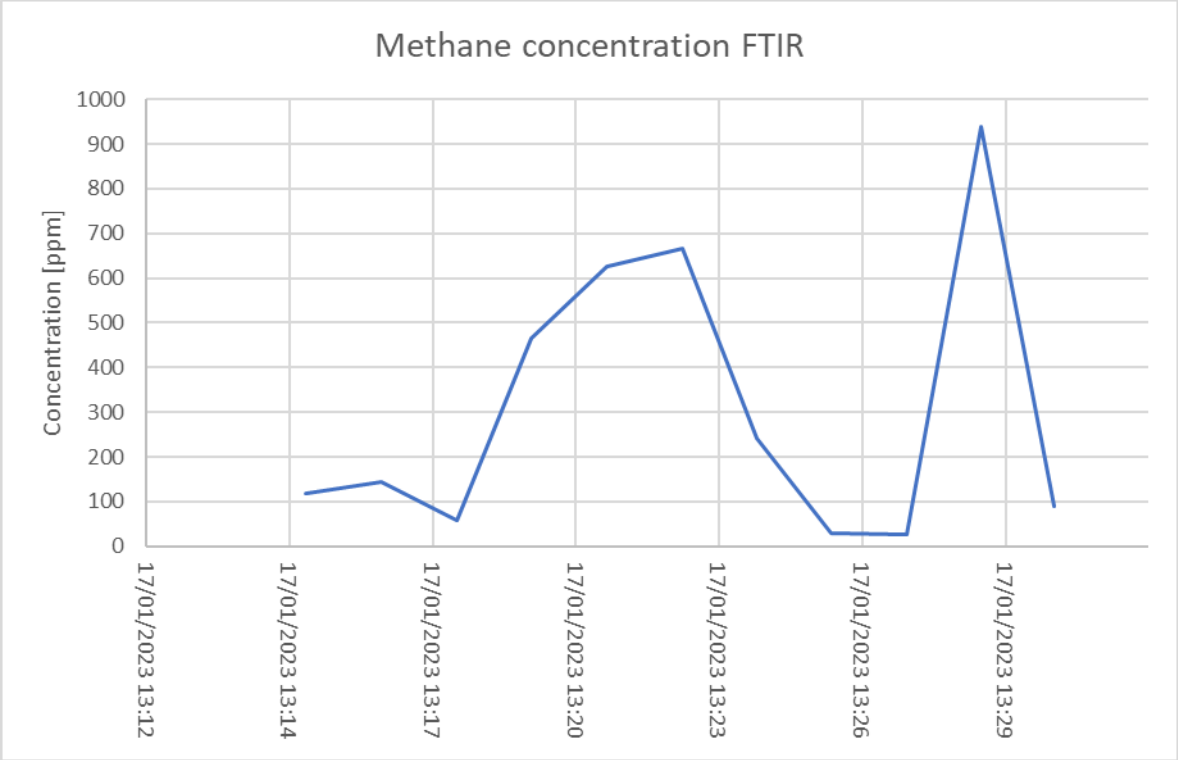


*Figure 38 - Methane concentration in correspondence of the torch using the FTIR.*

Regarding the closed part of the landfill, three main areas have been identified. They are reported in Figure 39. Unfortunately, aerial images have not updated yet. At the moment, this part of the landfill is a grassy hill with a height of 5 meters. The first part identified is at the edge of the hillock (yellow rectangles), the second one is on the right part of the site (red circle) and the third one is on the top of the hillock (orange circle). The different behaviour is probably due to the different types of coverage that have been used in the parts of the hill.

The average concentrations in these areas are respectively 4 ppm, 55 ppm and 10 ppm.

*Figure 39 – Depleted lot of the landfill.*

The behaviour of the concentration of methane in the outer side of the hill can be observed in Figure 40. The value of the concentration is considerable constant for most of the time. Getting closer to the hotspot, $CH_4$ concentration starts to increase, but a variation in the order of 1.5 ppm can be considered acceptable.

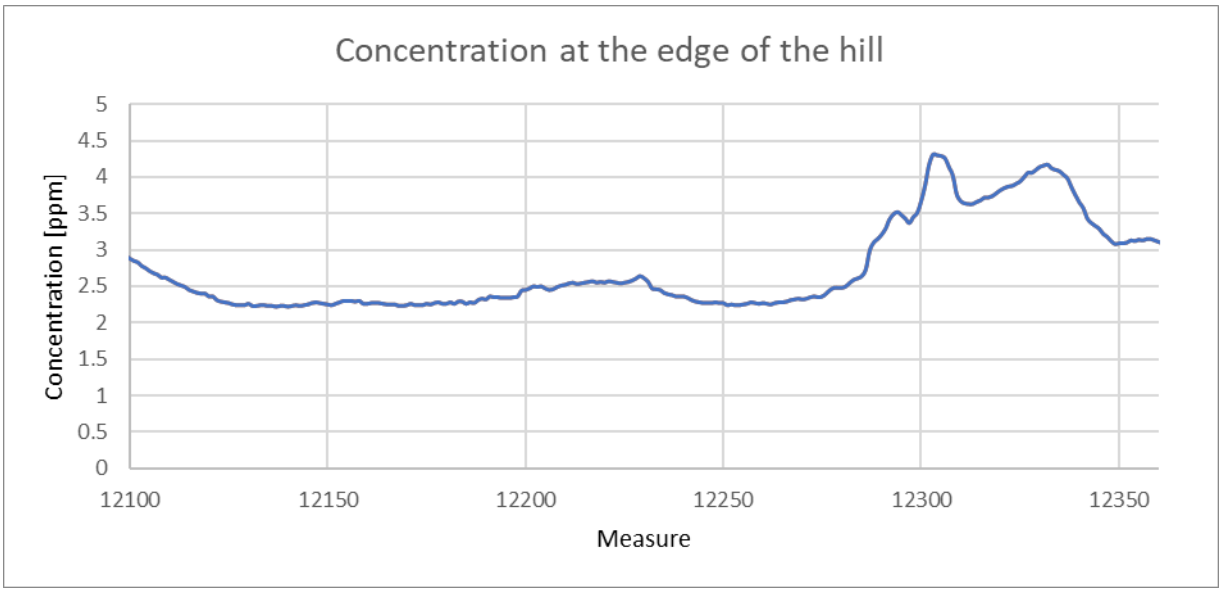


*Figure 40 - Methane concentration at the edge of the hill.*

On the right of the hill, there is the point that can be considered the hotspot of the area. Figure 41 shows that the variability of the concentration is very high. The peak of 260 ppm is difficult to explain. If as assumption the peak is justified by an error of the instrument and removed from the measurements, the average concentration in this area would be 49 ppm instead of 55 ppm. This particular part of the site should be better analysed using other instrumentations such as flux chambers to clearly identify the reason behind this behaviour.

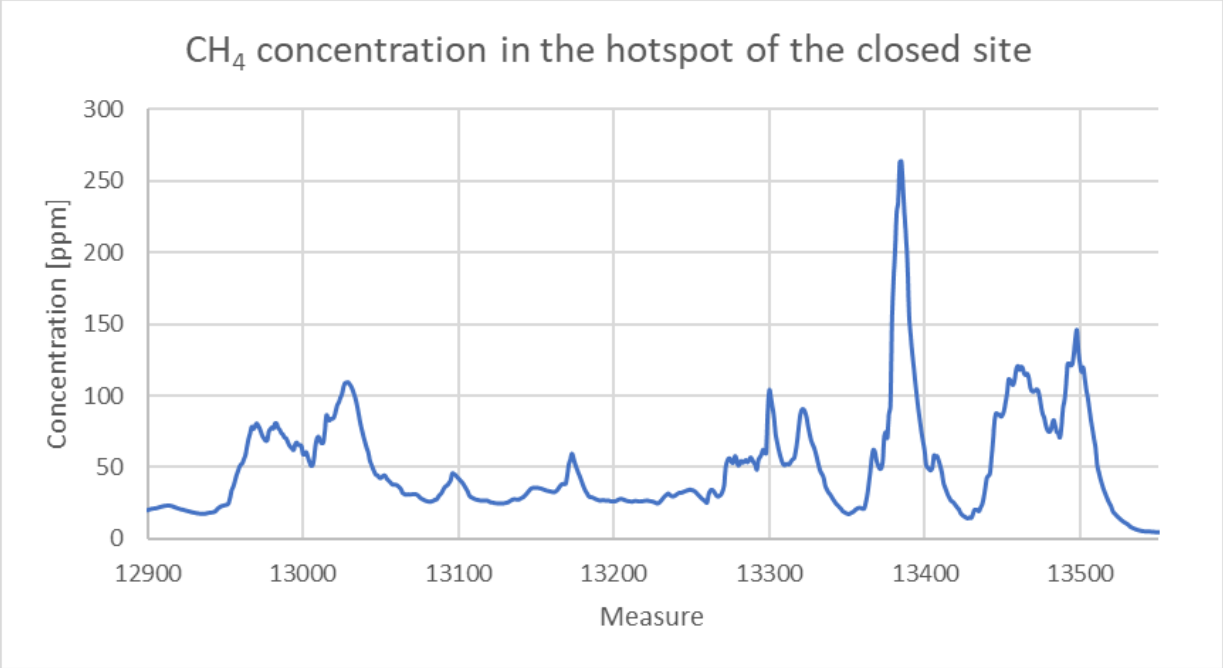


*Figure 41 - Concentration of methane in the right part of the hill.*

The variation of the concentration at the top of the hill can be observed in Figure 42. In this case too there is a peak difficult to be explained, but in general measures often remain in an interval between 5 and 15 ppm.

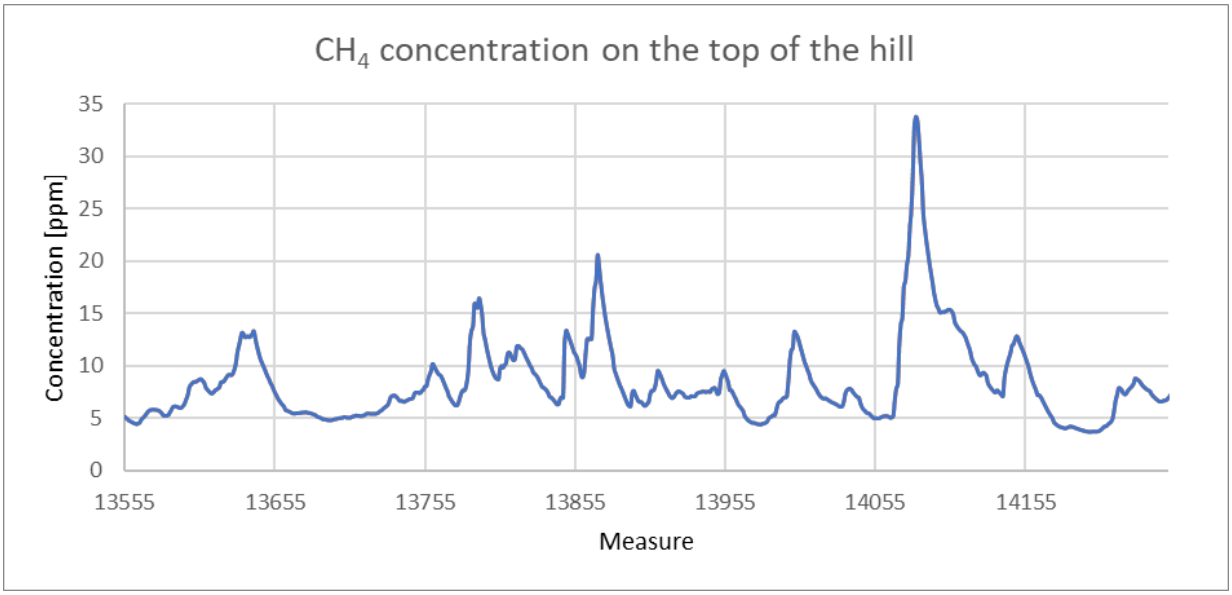


*Figure 42 - Methane concentration at the top of the hill.*

The “active” side of the landfill is divided into two parts. They are reported in Figure 43. Once again, the image is old and doesn’t represent the actual situation. The first one (yellow rectangle) is at the ground level, while the second one (red rectangle) is at a height of 3 meters. This part has been analysed with less accuracy than the part at ground level for safety reasons (machinery were working).

In this case, the average concentration of the two areas are respectively 7 ppm and 21 ppm. These values of concentrations have been calculated neglecting the torches. The difference in terms of concentration between the two parts could be explained by the working activity that was being carried out.

*Figure 43 - Active part of the landfill.*

The variation of the concentration in the ground level part of the site can be observed in Figure 44. The peaks due to the torches have been removed from the graph, setting the respective values equal to zero. The influence of these hotspots remains visible, especially in the last part of the graph, where the average value of $CH_4$ concentration is higher than in the rest of the graph.

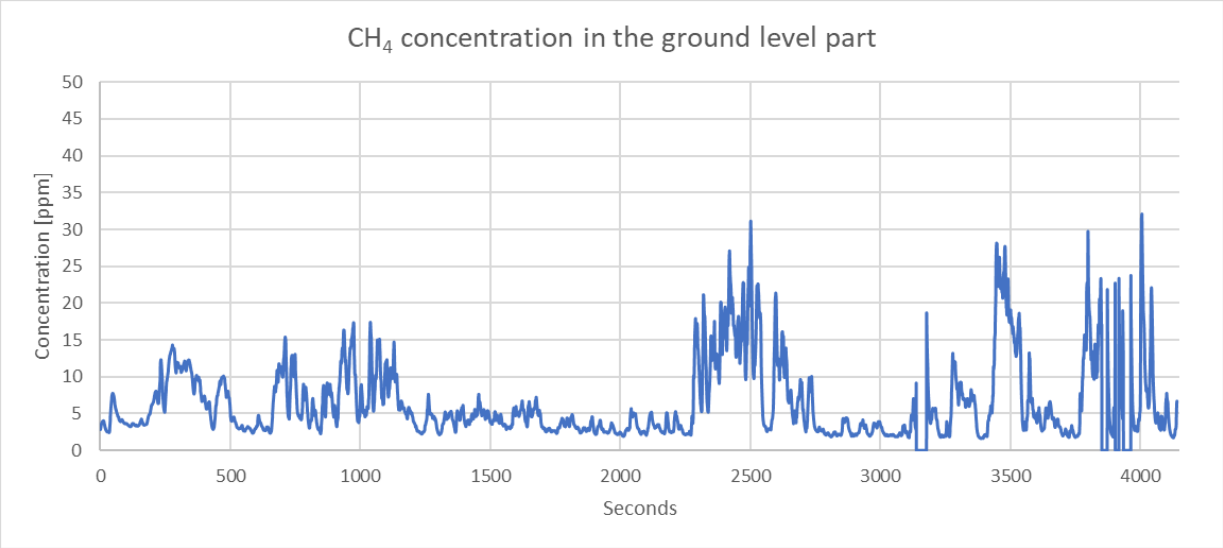


*Figure 44 - Methane concentration in the ground level part.*

The same process has been performed for the raised side of the active site. Results are shown in Figure 45. The variability of the concentration in this area is much higher than in the rest of the site. The influence of both torches and machinery doesn't allow to ensure the validity of these results. For the future, it would be interesting performing other measurements using instruments such as flux chambers in the area closer to the torches.

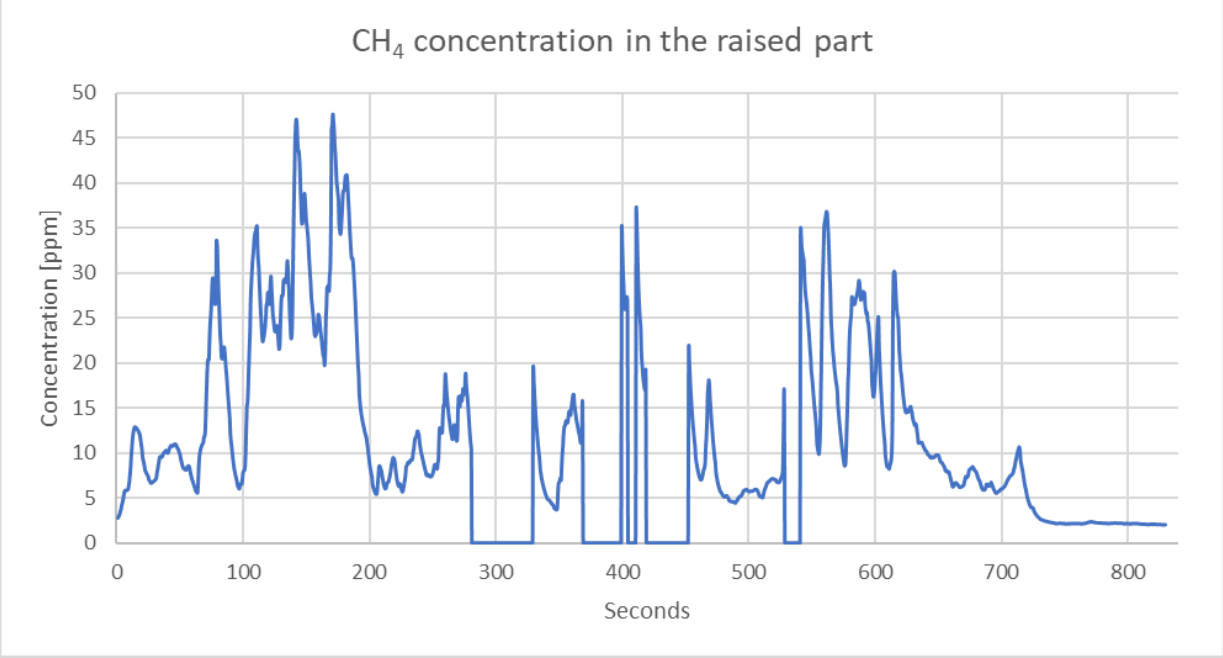


*Figure 45 - Methane concentration in the raised part..*

Once obtained the concentration of each point, a model has been created thanks to the software Surfer. The interpolation of the points has been obtained using Kriging. The result can be seen in Figure 46. Even if the torches have been removed from the model, their influence is clearly visible. It is important

to observe that the concentration of methane reaches levels comparable to the background one quickly. In fact, at the edges of the landfill in most cases the concentration is below 2 ppm. On the depleted lot it is highlighted once again the hotspot on the right of the hill, while in the left part the concentrations are between 2 and 10 ppm.

Unfortunately, data in the middle of the landfill have not been recorded, so it is not possible to say if the model fits well with the real situation or if there are present other hotspots that modify the gradient of the concentrations.

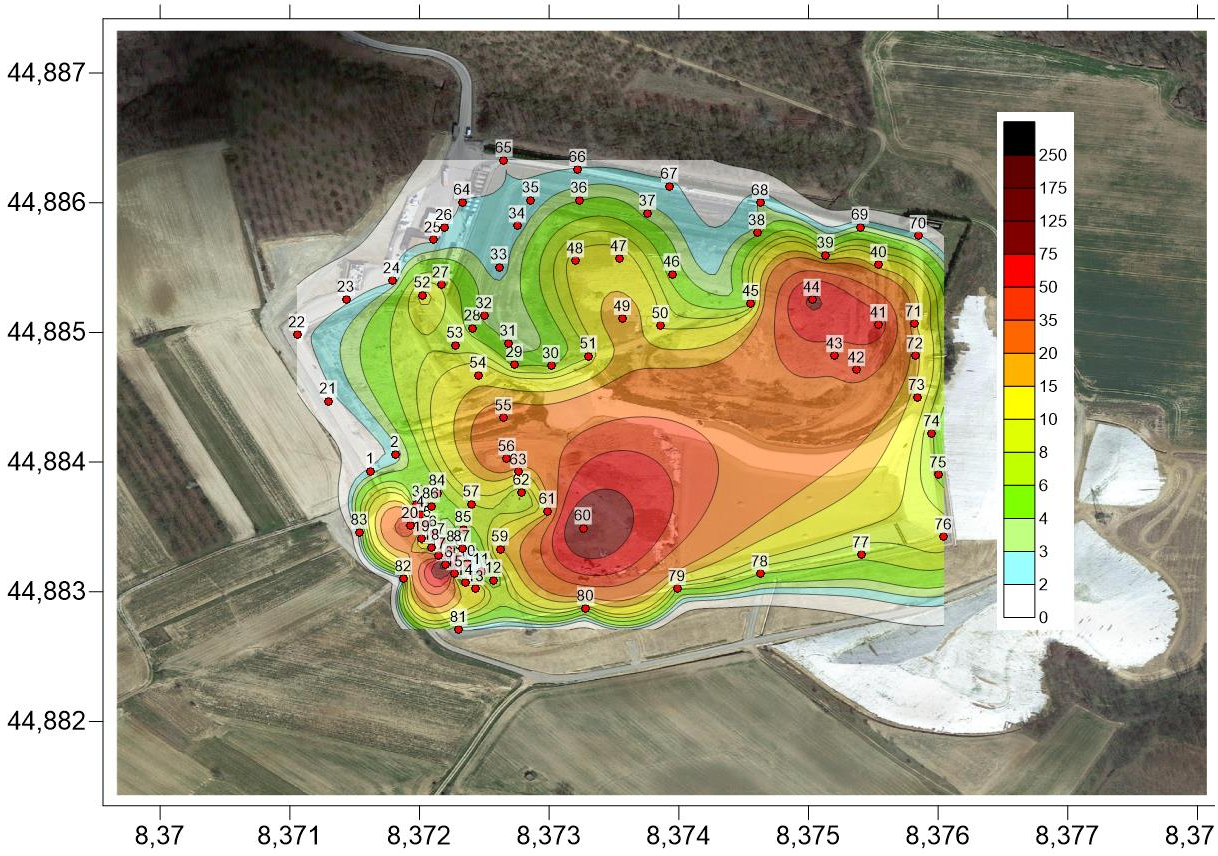


*Figure 46 - Methane emissions in the landfill.*

### 3.3.2 Comparison between $CH_4$ and $CO_2$ concentrations

TDLAS is not able to sample the concentration of $CO_2$. For this reason, the only data available come from the torch that has been analysed using the FTIR. As Figure 47 shows, the correlation between the two gases is evident.

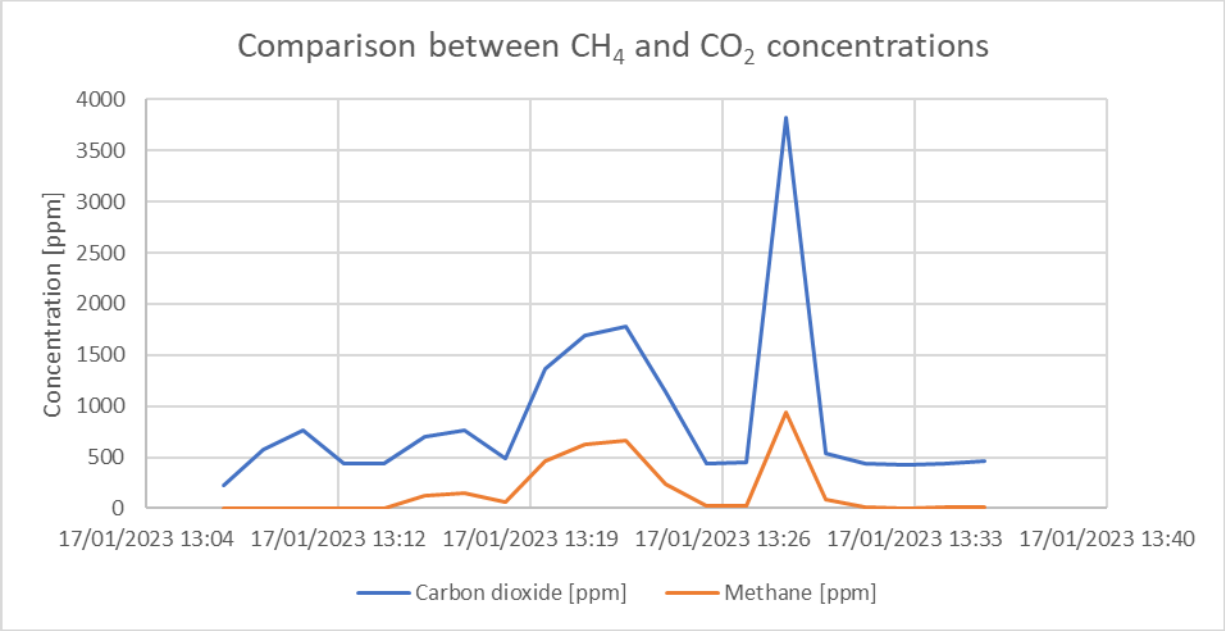


*Figure 47 - Comparison between $CH_4$ and $CO_2$ concentrations.*

Another way to observe the correlation between the two GHGs is based on a scatter plot. As visible from Figure 48, with the only exception of high value of concentrations of both gases (that are not reliable), the correlation is evident. The value of $R^2$=0.89 confirm the hypothesis.

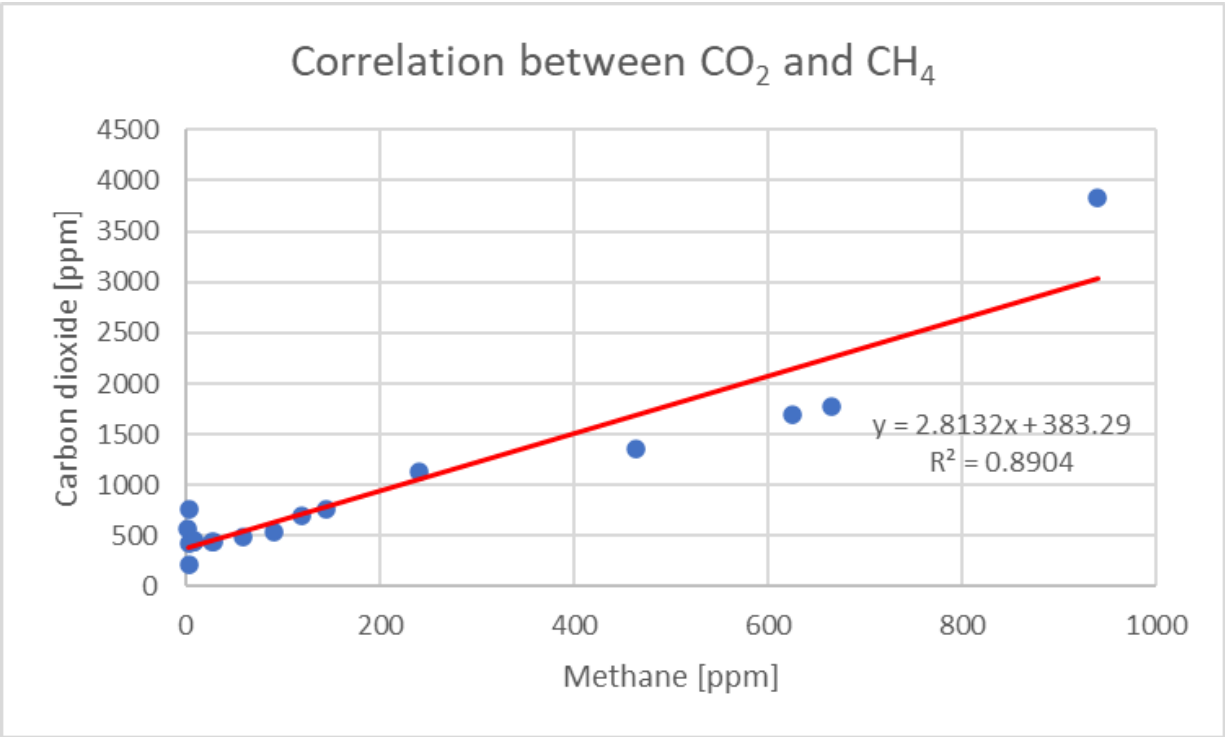


*Figure 48 - Correlation between $CO_2$ and $CH_4$.*

## 3.4 Lesson learnt and possible developments

From the discussion of the results, both the pros and the cons of the TDLAS technology emerge. The most relevant advantage of TDLAS is the possibility to get sample from the whole site in a fast and comfortable way. This technology could be used during a screening campaign, focusing on the identification of possible hotspots or points in which the concentration changes without apparent reasons. The main problems of this approach are related to the impossibility to obtain a value of the flux and to the limited range of detection of the instrument: as seen from the torches, a range of at least one order of magnitude higher is necessary.

# 4 Conclusions

This thesis presented the application of FTIR and TDLAS for methane emission measurement in two different case studies, an anaerobic digester and a municipal solid waste landfill.

The main advantage of FTIR turned out to be the possibility to detecting several gases in a single measurement. The spectra obtained can be then analysed using a specific software and understand if results are reliable or not. The instrument requires a considerable amount of energy that must be supplied by a battery. From the field, an 80 Ah battery lasted about 4 hours. The FTIR instrument can be transported by two persons, but its weight and its size make it challenging to use it in difficultly accessible sites. The suggested solution is to bring a long sampling tube and move the instrument the least possible. The best characteristics of TDLAS are its precision, portability, and sampling rate (two measures per second). It is a great tool to screen the whole site of interest getting reliable results. Moreover, an entire day of measurements doesn't require a recharge of the battery. Unfortunately, it can record only methane concentration and its measurement range (up to 100 ppm) can be too small for certain applications in the environmental field. For both the instruments, the integration of low-cost GPS systems proved acceptable for georeferencing measurements for environmental purposes, whereas different solutions should be considered for indoor or smaller-scale environments.

The use of FTIR and TDLAS concentration measurements for inverse modelling estimates of GHG fluxes proved challenging and hardly reliable. An attempt was made for the case study of the anaerobic digester close to a cattle barn, inferring a flux of 10.565 $tCH_4$/year, which is in the order of magnitude of those derived from literature studies. However, because of the strong assumptions related to the flat topography and to the constant speed and direction of the wind, other approaches should be used to guarantee a more precise calculation of the fluxes.

A possible suggestion to improve the results is the integration of a flux chamber into the setup. The combination of these three tools would be suggested because they would be well integrated with each other: TDLAS would be used to identify the points of interest of the site, the FTIR would be used to detect the eventual presence of other GHGs, and the flux chamber would be used to get the flux from the hotspots.

The use of UAVs has been often claimed as a solution to derive GHG fluxes on large scales. However, the concentration of methane in the case studies considered quickly declined with the distance from sources and hence the values measured are often hardly distinguishable from the background values. The use of drones would therefore be useful only if applied very close to the site. An interesting application of the drone would be the detection of the concentration of methane at several heights, but, in this case, it would be needed studies to understand the influence of the UAV's spinning blades. Moreover, the wind speed at defined heights from the ground should be known.

Thanks to the FTIR, another aspect that has been considered is related to the correlation between the concentration of methane and carbon dioxide. In the case of the biogas plant, because of the different states of the manure, it has not been possible to identify a clear correlation between the two gases ($R^2$=0.46). A more interesting result has been achieved analysing the MSW landfill. The value of $R^2$=0.89 obtained measuring the LFG that came out from the torches demonstrates that $CH_4$ and $CO_2$ are correlated. To better investigate this aspect, it could be useful to screen the whole site with a FTIR and, in case of positive correlation, repeat this methodology also in other MSW landfills.

In conclusion, this thesis demonstrates that FTIR and TDLAS are very useful tools to perform a preliminary survey of a site. The integration with one of the methods described in the first chapter would guarantee a precise and reliable idea of the emission levels of a site.

# References


[1] IPCC, IPCC Assessment Report 6 - Summary for Policy Makers, IPCC. (2021). https://bit.ly/IPCC_AR6_SPM (accessed January 30, 2023).

[2] IPCC, IPCC Special report - Summary for Policy Makers, IPCC. (2018). https://bit.ly/IPCC_Special_SPM (accessed January 30, 2023).

[3] L. Al-Ghussain, Global warming: review on driving forces and mitigation: Global Warming: Review on Driving Forces and Mitigation, Environ. Prog. Sustainable Energy. 38 (2019) 13–21. https://doi.org/10.1002/ep.13041.

[4] T.M. Letcher, Why do we have global warming?, in: Managing Global Warming, Elsevier, 2019: pp. 3–15. https://doi.org/10.1016/B978-0-12-814104-5.00001-6.

[5] D. Kweku, O. Bismark, A. Maxwell, K. Desmond, K. Danso, E. Oti-Mensah, A. Quachie, B. Adormaa, Greenhouse Effect: Greenhouse Gases and Their Impact on Global Warming, JSRR. 17 (2018) 1–9. https://doi.org/10.9734/JSRR/2017/39630.

[6] OurWorldInData, GHGs emissions in 2016, Ourworldindata. (2020). bit.ly/GHGs_emissions_OWD.

[7] EU, COMMUNICATION FROM THE COMMISSION TO THE EUROPEAN PARLIAMENT, THE COUNCIL, THE EUROPEAN ECONOMIC AND SOCIAL COMMITTEE AND THE COMMITTEE OF THE REGIONS on an EU strategy to reduce methane emissions, European Union. (2020). bit.ly/EU_Strategies (accessed January 20, 2023).

[8] J. Mønster, P. Kjeldsen, C. Scheutz, Methodologies for measuring fugitive methane emissions from landfills – A review, Waste Management. 87 (2019) 835–859. https://doi.org/10.1016/j.wasman.2018.12.047.

[9] C. Scheutz, R.B. Pedersen, P.H. Petersen, J.H.B. Jørgensen, I.M.B. Ucendo, J.G. Mønster, J. Samuelsson, P. Kjeldsen, Mitigation of methane emission from an old unlined landfill in Klintholm, Denmark using a passive biocover system, Waste Management. 34 (2014) 1179–1190. https://doi.org/10.1016/j.wasman.2014.03.015.

[10] C. Geck, H. Scharff, E.-M. Pfeiffer, J. Gebert, Validation of a simple model to predict the performance of methane oxidation systems, using field data from a large scale biocover test field, Waste Management. 56 (2016) 280–289. https://doi.org/10.1016/j.wasman.2016.06.006.

[11] H. Scharff, Martha, Rijn, Hensen, Flechard, Oonk, Vroon, de Visscher, Boeckx, A comparison of measurement methods to determine landfill methane emissions, (2003). bit.ly/Methods_Review (accessed January 31, 2023).

[12] R.A. Hashmonay, R.M. Varma, M.T. Modrak, R.H. Kagann, R.R. Segall, P.D. Sullivan, Radial Plume Mapping: A US EPA Test Method for Area and Fugitive Source Emission Monitoring Using Optical Remote Sensing, in: Y.J. Kim, U. Platt (Eds.), Advanced Environmental Monitoring, Springer Netherlands, Dordrecht, 2008: pp. 21–36. https://doi.org/10.1007/978-1-4020-6364-0_2.

[13] T. Clauß, T. Reinelt, J. Liebetrau, A. Vesenmaier, M. Reiser, C. Flandorfer, S. Stenzel, M. Piringer, A.M. Fredenslund, C. Scheutz, M. Hrad, R. Ottner, M. Huber-Humer, F. Innocenti, M. Holmgren, J. Yngvesson, Recommendations for reliable methane emission rate quantification at biogas plants, DBFZ, 2019. bit.ly/CH4_BIOGAS.

[14] Charlotte Schuetz,*, J. Bogner, J. Chanton, D. Blake, M. Morcet, P. Kjeldsen, Comparative Oxidation and Net Emissions of Methane and Selected Non-Methane Organic Compounds in Landfill Cover Soils, Environ. Sci. Technol. 37 (2003) 5150–5158. https://doi.org/10.1021/es034016b.

[15] J.J.A. Lozeman, P. Führer, W. Olthuis, M. Odijk, Spectroelectrochemistry, the future of visualizing electrode processes by hyphenating electrochemistry with spectroscopic techniques, Analyst. 145 (2020) 2482–2509. https://doi.org/10.1039/C9AN02105A.

[16] M.B. Frish, R.T. Wainner, M.C. Laderer, K.R. Parameswaran, D.M. Sonnenfroh, M.A. Druy, Precision and accuracy of miniature tunable diode laser absorption spectrometers, in: M.A. Druy, R.A. Crocombe (Eds.), Orlando, Florida, United States, 2011: p. 803209. https://doi.org/10.1117/12.884526.

[17] EPA, EPA Handbook: Optical and Remote Sensing for Measurement and Monitoring of Emissions Flux of Gases and Particulate Matter, EPA. (2018). bit.ly/EPA_Guide (accessed January 30, 2023).
[18] Axetris, Axetris, Axetris. (n.d.).
[19] A.P. Ravikumar, J. Wang, A.R. Brandt, Are Optical Gas Imaging Technologies Effective For Methane Leak Detection?, Environ. Sci. Technol. 51 (2017) 718–724. https://doi.org/10.1021/acs.est.6b03906.
[20] M. Hrad, M. Huber-Humer, T. Reinelt, B. Spangl, C. Flandorfer, F. Innocenti, J. Yngvesson, A. Fredenslund, C. Scheutz, Determination of methane emissions from biogas plants, using different quantification methods, Agricultural and Forest Meteorology. 326 (2022) 109179. https://doi.org/10.1016/j.agrformet.2022.109179.
[21] IEA, An introduction to biogas and biomethane, IEA. (n.d.). bit.ly/BIOGAS_IEA.
[22] WeatherUnderground, Weather, WeatherUnderground. (2022). bit.ly/Weath_23_12.
[23] O.A. Castelán-Ortega, J. Carlos Ku-Vera, J.G. Estrada-Flores, Modeling methane emissions and methane inventories for cattle production systems in Mexico, Atmósfera. 27 (2014) 185–191. https://doi.org/10.1016/S0187-6236(14)71109-9.
[24] K.A. Johnson, D.E. Johnson, Methane emissions from cattle, Journal of Animal Science. 73 (1995) 2483–2492. https://doi.org/10.2527/1995.7382483x.
[25] EPA, LFG Energy Project Development Handbook, EPA. (2020). bit.ly/EPA_LFG (accessed January 20, 2023).
[26] U. Lee, J. Han, M. Wang, Evaluation of landfill gas emissions from municipal solid waste landfills for the life-cycle analysis of waste-to-energy pathways, Journal of Cleaner Production. 166 (2017) 335–342. https://doi.org/10.1016/j.jclepro.2017.08.016.
[27] G. Tassielli, B. Notarnicola, P.A. Renzulli, R. Di Capua, M. De Molfetta, D. Fosco, Screening via drone di una discarica di RSU per la ricerca dei punti di emissione di metano, (n.d.). bit.ly/UAV_RSU_screen.
[28] IPCC, IPCC Guidelines for National Greenhouse Gas Inventories, IPCC. (2006). bit.ly/IPCC_TFI_2006 (accessed January 31, 2023).
[29] J. Bogner, M. Meadows, P. Czepiel, Fluxes of methane between landfills and the atmosphere: natural and engineered controls, Soil Use & Management. 13 (1997) 268–277. https://doi.org/10.1111/j.1475-2743.1997.tb00598.x.